Development of Porous Silicon Membranes with Hydrophobic Vapor Traps to Desalt Hydraulic Fracturing Flowback Water

James Lazenby

The Ohio State University

A thesis submitted for

Undergraduate Honors Research Distinction in Mechanical Engineering

4 April 2019

Acknowledgments

I would like to thank Dr. Shaurya Prakash for his advice and guidance throughout the duration of this project, as well as his mentorship, which has refined my engineering skill-set and future ambitions. I would also like to thank Dr. Kaushik Rangharajan and Prashanth Mohana Sundaram, who have been additional mentors and have also provided assistance throughout this project. I further extend this thank you to all members of the Microsystems and Nanosystems Lab at OSU.

Abstract

In 2017 the United States consumed 98 quadrillion BTUs of energy, but only produced 88 quadrillion BTUs of energy domestically. This has amplified the United States' reliance on foreign entities for energy imports and induced high volatility in the energy market. Consequently, there is a need for localized, cost-effective energy sources, which has resulted in numerous unconventional oil and gas production methods, including hydraulic fracturing. During the hydraulic fracturing process, an estimated 3-5 million of gallons of water per well are pumped into the rock bed to generate fissures in the surrounding rock in order to extract the underlying hydrocarbons. Approximately 20-40% of this water flows back to the surface in 60 days with a hyper-saline composition that can be 3-10 times saltier than seawater. Moreover, flowback water, depending on the geographical location, contains heavy metals, organic contamination, and possible radionuclides. Currently, flowback water disposal occurs commonly through deep well injection, as no reliable flowback water treatment methods presently exist.

One possible method to desalinate hydraulic fracturing flowback water is through the use of hydrophobic vapor traps. Proof-of-concept experiments with three nanochannels in silica of length 32 μm and at a pressure of 48 bar, containing hydrophobic sections have been able to achieve an average desalting of 95% in 20 minutes using a 5 M NaCl draw solution. This project outlines the development of porous silicon membranes with hydrophobic vapor traps, as a possible strategy to scale-up the proof-of-concept demonstration to viable laboratory evaluation of desalination of flowback water using forward osmosis.

The main deliverables of this project include the successful development and validation of a porous silicon recipe process. Additionally, the design and fabrication of a porous silicon membrane for transport testing is also documented.

The fabricated porous silicon membranes had 10 ± 2.2 nm diameter pores and a pore surface density of 23.05%. The pore size and pore distribution were based on image analysis of scanning electron microscopy (SEM) imaging. The porous silicon membranes were tested in the custom designed and built permeation set-up to show that membranes of diameter 1.2 cm and thickness 10 ± 1.3 μm were able to sustain osmotic gradients of 4.825 atm and demonstrate transport of water across the nanopores. It was determined that non-functionalized membranes, during a 24-hour period, were able to desalt a 100 mM NaCl solution by, 24.25 ± 1.63%.

Table of Contents

List of Figures

List of Tables

Chapter 1

Introduction and Objectives

This section overviews the United States' energy production and consumption and introduces the motivation for a high-flux, low-cost hydraulic fracturing flowback membrane that can be used in an overall desalination system. Moreover, limitations of existing technologies are presented and an overview of porous silicon as the choice for material for this work is also discussed.

1.1 Need for localized energy independence

In 2017, The United States produced 88 quadrillion BTUs of energy [1]. However, during this same period, the Unites States consumed 98 quadrillion BTUs of energy. This resulted in a 10 quadrillion BTU disparity, which is commonly referred to as the energy deficit. In order to compensate for the lack of sufficient domestic energy production, the Unites States imports energy resources, normally in the form of crude oil. Importing energy resources, directly influences the American consumer through volatile prices, dependence on other countries, and continued reliance on outdated energy technologies [2]. Thus, there has been substantial interest throughout the United States, to promote localized energy independence, by effectively exploiting the natural resources of a locality's region.

In some instances, this manifests in the form of solar and wind power, but throughout the Appalachian Basin, it takes the form of unconventional oil and gas production methods. Figure 1, examines how primary energy projection sources have changed over time, due to an increase in energy demands and new technologies. In 1950, the Unites States produced 25.5 quadrillion BTUs of energy in the form of coal and crude oil. At that time, this amounted to 71.7% of all energy produced in the Unites States. However, over time the United States began to explore other energy sources. In 2017, natural gas and natural gas plant liquids (NGPL) were increasingly important to the total contribution to energy sources accounting for 32.9 quadrillion BTUs produced. This corresponds to 37.6% of all energy produced in 2017 in the United States.

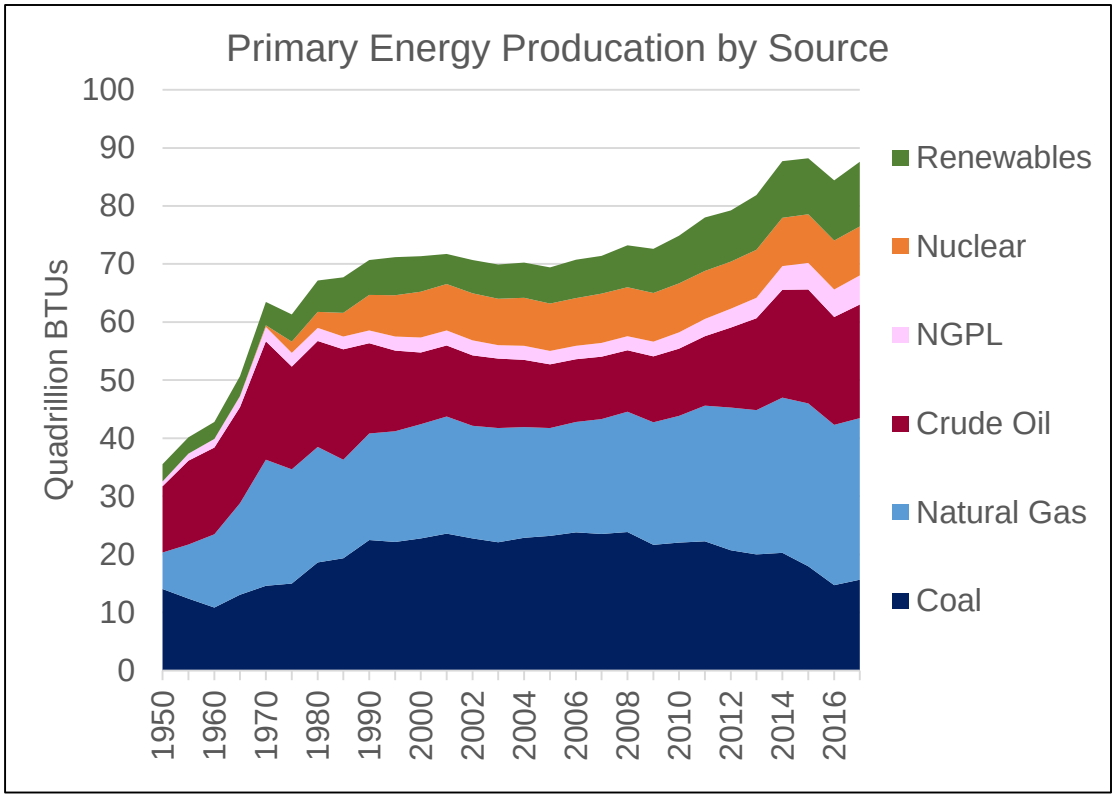

Figure 1: The United States' energy production sources [1].

1.2 Hydraulic fracturing and the horizontal drilling process

Natural gas is a naturally occurring hydrocarbon that forms under the surface of the earth when organic matter is heated and compressed [3]. Natural gas is stored in the rock formations and is commonly found next to coal and oil deposits. The access and capture of natural gas occurs though a process known as hydraulic fracturing, which is colloquially referred to as "fracking."

The hydraulic fracturing of reservoirs to collect natural gas is one of the unconventional energy production methods that has garnered interest. Throughout the United States, hydraulic fracturing has expanded prolifically, with 1,869 operational wells in Ohio as of 2017 [4]. This is not surprising because the Marcellus Shale reservoir, which encompasses New York, Pennsylvania, Ohio, and West Virginia, has been estimated by the U.S. Geological Survey (USGS) to hold more than 1.43 trillion cubic meters of recoverable gas in the Devonian rock layer [5]. This is enough recoverable natural gas, to power all domestic natural gas power plants for 5.4 years [6]. The

Devonian layer also includes the Utica Shale and New Albany Shale reservoirs, which contain additional recoverable gas.

The focus in this honors thesis is in evaluating methods for treating flowback water from the extraction of natural gas through a process referred to as hydraulic fracturing. The hydraulic fracturing process is briefly described next, with a schematic depiction in Figure 2.

First, a vertical wellbore is drilled to the depth of the targeted rock layer, which is typically between 5,000 – 12,000 ft from the surface [7]. Then, the wellbore is extended horizontally, normally for an additional 2,000 ft, in a process known as directional drilling [7]. The horizontal wellbore increases the amount of contact with increased surface area between well bore and rock formation and allows more natural gas to be collected per well. Once the wellbore is drilled, 3-5 million gallons of high pressure fracking fluid are pumped into the well bore [8]. The fracking fluid comprises predominantly water but contains large qualities of hydrochloric acid, friction reducers, and surfactants, which are responsible for dissolving minerals, decreasing friction at the fluid-pipe interface, and increasing the viscosity of the fracking fluid [9]. The high pressure fluid then creates fissures in the surrounding rock. These fissures are held open by the proppants, normally sand, which are also in the fracking fluid [9]. The natural gas is then released from the fractured rock and can escape to the surface for refinement and collection.

However, after the drilling process, 10-40% of the drilling fluid flows back to the surface within 60 days [9, 10]. This flowback water is usually a hyper-saline (brine) solution, which poses significant treatment and disposal challenges. Table 1 details the composition of hydraulic fracturing flowback waste and how it differs between shale formations. Table 2 contains the concentration of typical constituents in hydraulic fracturing fluid.

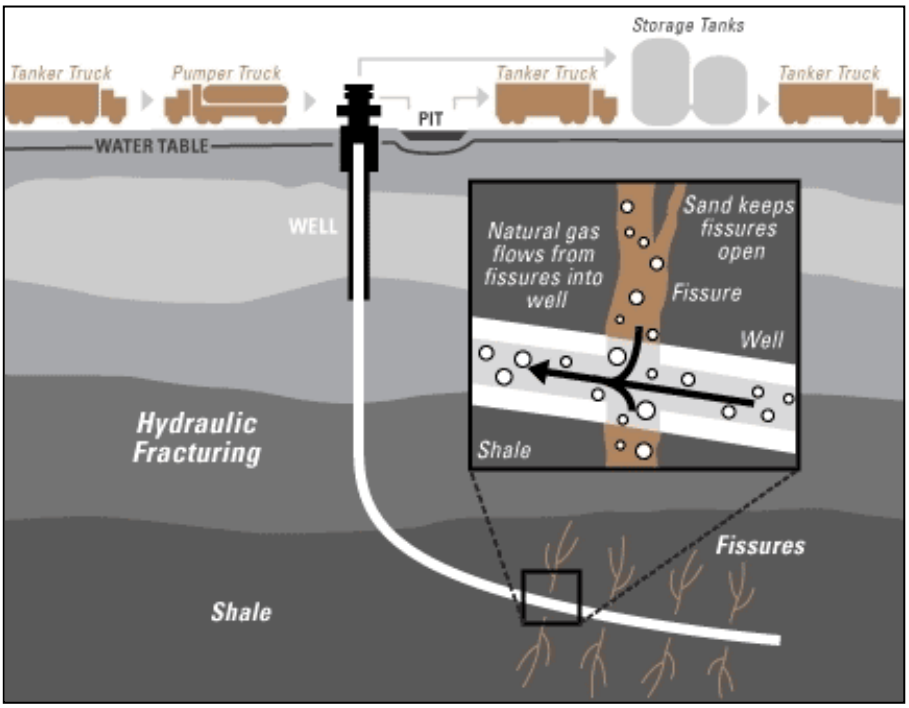

Figure 2: Overview of the hydraulic fracturing process [11].

Table 1: Inductively-coupled plasma mass spectrometry (ICP-MS) and Ion-chromatography was used to quantify ionic composition of Utica shale flowback. Composition of the Barnett and Haynesville formations was obtained from past reports [8].

Content	UTICA	Barnett (Tx)	Haynesville (Tx)
TDS	183,333.33	40,000-185,000	40,000-205,000
Na^{+}	48,998.67 ± 169.7	10,000-47,000	15,000-55,000
Ca^{2+}	15,105.67 ± 116.0	220-20,000	3,100-3,4000
Mg^{2+}	1,793.13 ± 9.8	200-3000	600-5,200
K^{+}	642.67 ± 2.7	4-216	NA
Sr^{2+}	4,003.55 ± 46.3	350-3,000	100-3,000
Ba^{2+}	1,235.41 ± 6.8	30-500	100-2,200
Cl^{-}	122,410.15 ± 3,214.6	25,000-110,000	20,000-105,000
Br^{-}	1,329.50 ± 46.6	34.3-532	NA
SO_4^{2-}	112.16 ± 0.4	15-200	100-400
PO_4^{3-}	20.41 ± 1.5	NA	NA

Table 2: The concentration of typical constituents in hydraulic fracturing fluid [8].

Function	Chemical	Max. Ingredient Function % by Mass
Carrier/Base Fluid	Freshwater	85.47795%
Proppant	Crystalline silica	12.66106%
Acid	Hydrochloric acid in water	1.29737%
Gelling Agent	Petroleum distillate blend	0.14437%
	Polysaccharide blend	0.14437%
Cross-linker	Methanol	0.04811%
	Boric acid	0.01069%
Breaker	Sodium chloride	0.04252%
Friction Reducer	Petroleum distillate, hydrotreated light	0.01499%
pH-adjusting Agent	Potassium hydroxide	0.01268%
Scale Inhibitor	Ethylene glycol	0.00540%
	Diethylene glycol	0.00077%
Iron Control Agent	Citric acid	0.00360%
Antibacterial Agent	Glutaraldehyde	0.00200%
	Dimethyl benzyl ammonium chloride	0.00067%
Corrosion Inhibitor	Methanol	0.00142%
	Propargyl alcohol	0.00010%

1.3 Current flowback water disposal methods

Hydraulic fracturing flowback water, is a hyper saline solution that is on average six times saltier than sea water [8]. Utica Shale flowback water has been extensively analyzed by our team and has been determined to have a total dissolved solids (TDS) content of 185,000 ppm, which in contrast to seawater has an average of 35,000 ppm and the hypersaline brine classification which has a minimum value of 60,000 ppm. This high salinity is problematic because these flowback waters are not treatable by current wastewater treatment plant (WWTPs), which are designed to remove total suspended solids (TSS) instead of TDS [5]. It is interesting to note that prior to 2008, the primary flowback water disposal method was treatment through WWTPs. However, after observing a 200% increase in TDS of nearby water sources, regulatory enforcement was enacted to limit the discharge at a maximum value of 500 ppm severely restricting the ability of WWTPs to treat flowback water for either re-use or disposal [12].

Moreover, desalination through the use of reverse osmosis (RO) membranes or conventional thermal process are not feasible. First, reverse osmosis membranes are not able to immediately treat the flowback water that is directly ejected from the well due to the high level of particulates requiring significant pre-treatment to reduce membrane fouling and scaling. All RO membranes are typically designed and engineered to treat seawater and the current RO membranes are unable to withstand the hydraulic pressure required for 50% desalting of 70,000 ppm solutions [12, 13, 14]. Conventional thermal desalination technologies, such as multistage flash and multiple effect distillation, have also been determined as impracticable. This is due to the high cost, large footprint, and difficulty required to transport between wells [12].

Thus, current well operators have resorted to disposing of flowback water by deep well injection. This process involves transporting wastewater to decommissioned wells, and injecting the solution back into the ground [15]. Re-injection is expensive, and costs on average $1-$6 per barrel to transport to the disposal well and $0.5 - $2.5 per barrel to re-inject [16]. This amounts to $47,000 – $400,000 total per well [15].

The re-injection of flowback water may also have detrimental environmental consequences with correlations established to local seismic events [17]. The scientific basis for these correlations proposes is that re-injected flowback water reduces the friction along fault formations which results in human induced seismic activity [17]. Furthermore, the re-injection of flowback water means millions of gallons of water are lost from the immediate environment surrounding the well site. In most cases the water required for drilling is obtained from nearby natural water resources. Removing this water from the environment may have a detrimental impact on the surrounding ecosystem and results in a net loss of useful water depending on the geographical location.

In Ohio, the total name plate capacity of all existing power plants is 13.05 GW [18]. Total name plate capacity is the maximum power which a power plant is capable of generating. In reality, the normal operating conditions of power plants are less than their total name plate capacity. However, due to increasing energy demands, there is an additional 7.66 GW of natural gas power plants proposed and under construction in Ohio [18]. Therefore, it is inevitable that a significant portion

of Ohio's future energy needs will be reliant on natural gas. Figure 3 overlays Ohio's well and utility geography. It can be observed that active wells and disposal wells are in close proximity and are predominantly located on top of the Utica shale basin. Additionally, it can be observed that existing power plants are located close to highly populated cities, while the proposed power plants will be located next to cities closer to the well sites. Furthermore, a strong correlation between disposal well locations and earthquake epicenters can also be observed [18].

Therefore, it is reasonable to expect natural gas production via hydraulic fracturing to continue for the foreseeable future with generation of significant flowback water. Consequently, if the need for a cost-effective realizable filter to treat hydraulic fracturing flowback water can be developed, it is likely that the process of hydraulic fracturing is more amenable as a responsible energy production practice.

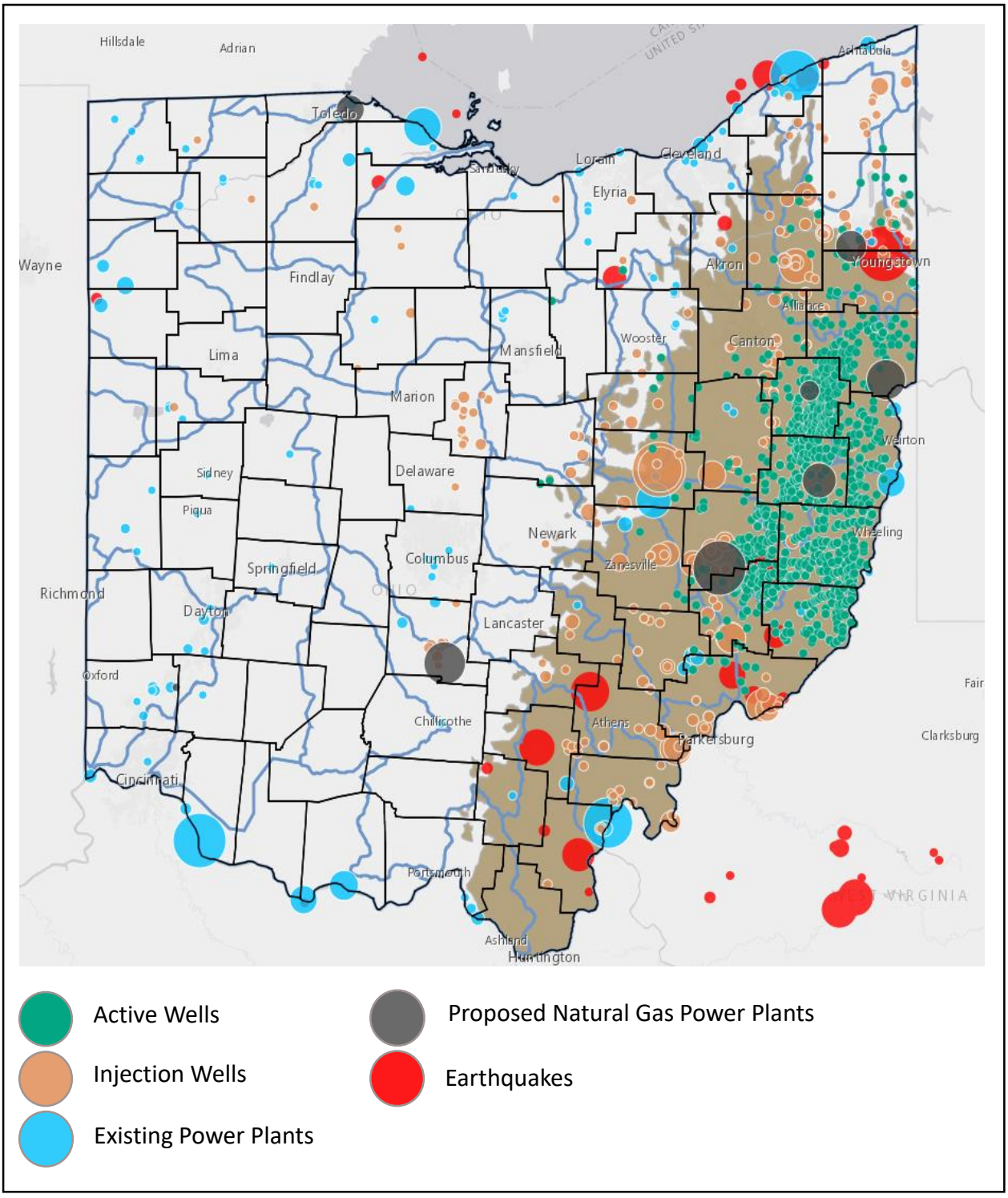

Figure 3: Map of Ohio, detailing active well sites, injection wells, existing and proposed power plants, and earthquakes [18].

1.4 The water-energy nexus

Energy production, in general, is a water intensive process. Energy and water are inherently interlocked, with water being a key component in cooling coal, gas, and nuclear power plants, mining natural energy resources, cleaning and washing equipment, and refining oil and gas for eventual energy use [8]. Coupled with competition from the agricultural industry, public supply, manufacturing industry, aquaculture, etc., demand for fresh water resources are at an all-time high. Consequently, this global challenge is referred to as the water-energy nexus.

Figure 4 displays the percentage of total freshwater withdrawals for a range of industries and applications. As can be seen, thermoelectric power generation is the largest withdrawer with >40% of total water withdrawals being used for power plant cooling processes [19]. In Figure 4, 'mining' encompasses the water used for the hydraulic fracturing process, while 'thermo-electric' includes water consumed by natural gas power plants.

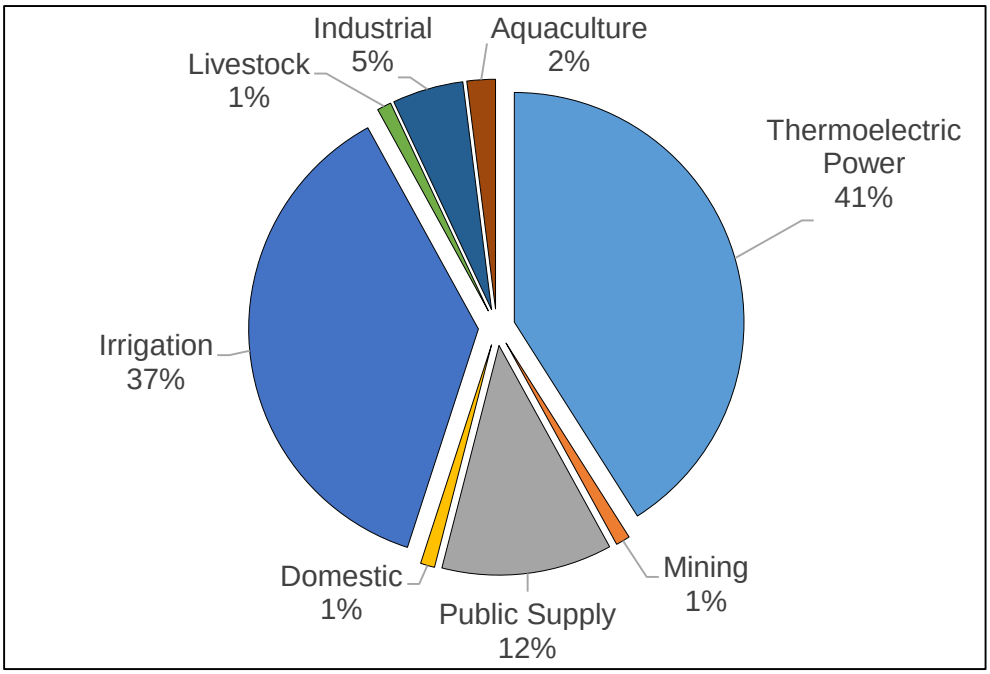

Figure 4: Percentage of total freshwater withdrawal used by certain industries and applications as estimated by a 2015 USGS report [19].

The water-energy nexus reveals itself in many different ways, such as water scarcity and water quality issues, and is highly dependent on the location [20]. The United States not only utilizes many different energy generation methods, but also implements a variety of water technologies to

accommodate freshwater demand in water scarce regions. The Southwest region of the United States, especially Arizona, is a unique area which boasts tremendous water-scarcity but generates >65% of the region's electricity generation from hydrocarbon-based power plants [21]. In Arizona, the lack of water is combated by the Central Arizona Project (CAP), which is a 336-mile aqueduct that is maintained with water from the Colorado river [20] It is interesting to note that the CAP is the largest consumer of energy in Arizona, due to the high pumping costs [20].

In the Central and Eastern areas of the United States, where water scarcity is not a defining issue, the water-energy nexus is more concerned with the quality of water. Coal mining has been the dominant industry in Appalachia since the early 1900s [20]. However due to the rush and sudden influx of mining towns during this period, adequate water infrastructure was not built. This has resulted in the contamination of drinking wells, landslides, and ecological damage, which are still prevalent today [20]. This water quality issue is also apparent in the Northeastern and Central areas of the United States which are dominated by hydraulic fracturing [20]. The water quality concerns connected to energy development and use is seen in Figure 5, which overlays the water-energy nexus with regions in the United States.

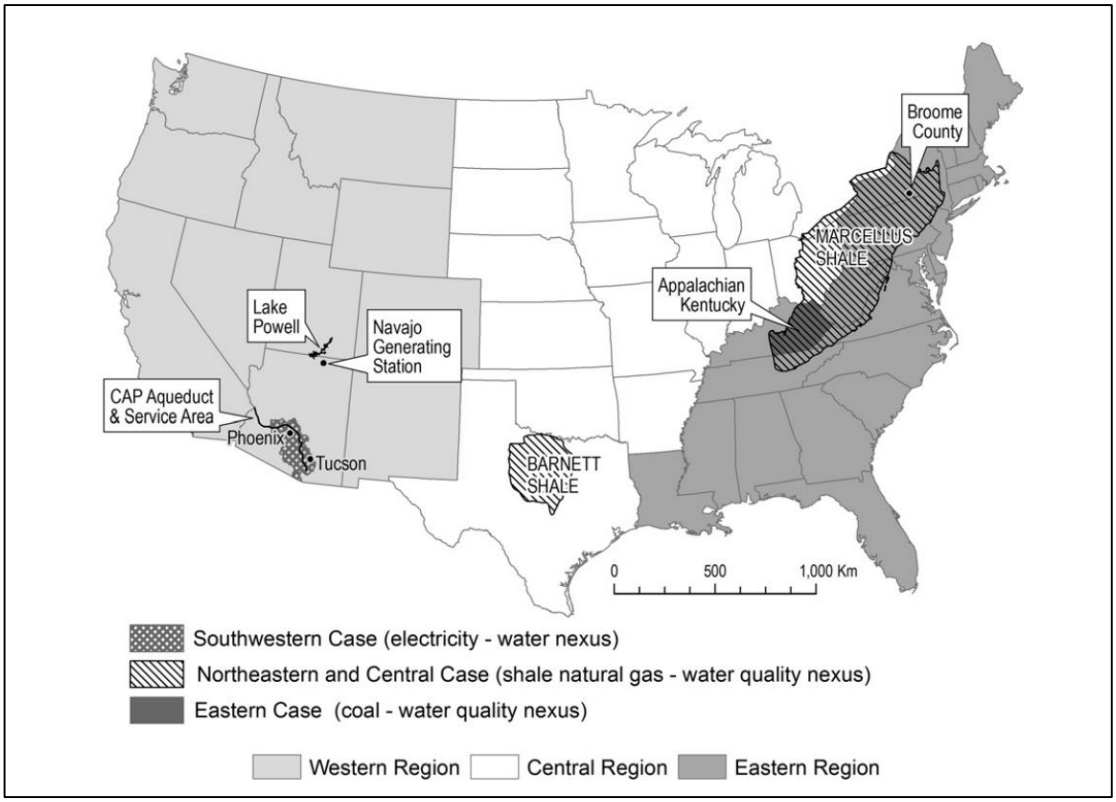

Figure 5: Water-energy nexus throughout the United States [20].

1.5 Proof of concept using nanochannels

To treat the hydraulic fracturing flowback water, one goal is to develop strategies to desalinate the source water enabling either re-use or a secondary treatment by WWTPs. Therefore, as part of this thesis two goals were pursued. First, is to extract usable water from the flowback to dilute other hard-to-treat industrial waters; second, gray water sources which also typically add burden of treatment to WWTPs or the natural environment [8, 22, 23, 24, 25, 26]

As a mode of desalination for this project, we chose to work with forward osmosis (FO) due to the relative low risk of membrane fouling compared to RO and also the ease of setting up experiments with high concentration of TDS in the source water obviating the need for external pumps driving flows for adequate pressure generation [27]. Our group, recently demonstrated a new way to use FO for desalinating hypersaline waters utilizing hydrophobic vapor traps [28]. Briefly, a portion of the fluid conduit responsible for water treatment (e.g., a pore in a membrane or a nanochannel in our proof-of-concept system, Figure 6) was rendered hydrophobic by chemical treatment [28]. The liquid water is unable to cross the hydrophobic barrier. As the goal is to use FO, we main a high osmotic pressure gradient across this hydrophobic trap, causing liquid water to evaporate from regions of low salt concentration and condense to regions of high salt concentration leading to an isothermal evaporation-condensation cycle driven by the osmotic pressure gradient.

As salt concentration within a solution increases, the vapor pressure of that solution decreases. Thus, when solutions of different molarities are separated by a hydrophobic barrier, a pressure gradient will occur. Success with small-scale, proof-of-concept experiments which utilized three hydrophobic vapor nanochannels, of length 32 μm and at a pressure of 48 bar, have been able to achieve an average flux of 47.3 $Lm^{-2}h^{-1}$ [28]. This resulted in an average desalting of 95% in 20 minutes using a 5M NaCl draw solution in a 12nl reservoir. A set-up of the system can be seen in Figure 6. By determining the treatment rate per pore, it was calculated that 1.3 trillion pores would be needed to treat 3 million gallons of flowback water during a 30-day period.

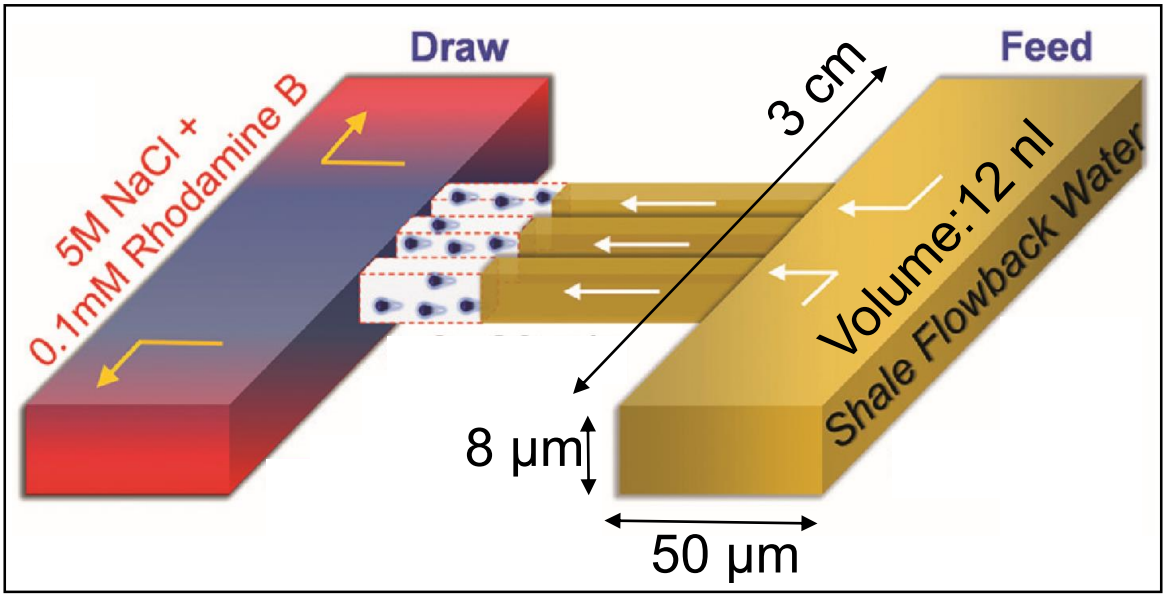

Figure 6: Schematic of three nanochannel set up that resulted in 95% desalting of draw solution after 20 minutes [28].

It is worth noting that in order to desalinate flowback water, a solution with a higher molarity must be used as the draw solution. Possible sources of this draw solution include agricultural run-off, and water produced from manufacturing plants. Table 3 compares the TDS of hydraulic fracturing flowback with other wastewaters, and outlines the dominant components in each stream. The benefits of diluting another contaminated water source are extensive. The proposed desalination method allows the composition and concentration of the solution to be controlled. Dilution, for instance, could result in a solution that is now filterable by current wastewater treatment plants or even a solution that is now clean enough for another industrial processes. What is specifically significant about dilution via hydrophobic vapor traps, is that it removes previous size and time constraints as apparent with a flux value of 47.3 $Lm^{-2}h^{-1}$.

Table 3: Wastewater streams with high TDS.

Wastewater Origin	TDS	Dominate Waste Component	Ref
Utica Shale Flowback	179,000-187,000	Heavy metals, Organic compounds, Radionuclides	N/A
Marcellus Shale Flowback	80,500		8
Barnett Shale Flowback	40,000-185,000		8
Haynesville Shale Flowback	40,000-205,000		8
Textile Industry	500-18,000	Sodium, Heavy Metals	22
Tannery	22,000-80,000	Organic Compounds, Chromium, Sulfide	23
Distillery	52,000-112,000	Organic Compounds	23
Chemical Manufacturing	31,000-35,000	Chlorine, Bromine, Sulfate	24
Pharmaceutical Manufacturing	2,300-2,700	Organic compounds	25
Agricultural Runoff	1,500-2,600	Nitrogen, Phosphorous	26

1.6 Overview of thesis and porous silicon

The purpose of this project is to scale-up the proof-of-concept desalination method by fabricating a porous silicon membrane with billions of nanopores, and to determine if similar flux values can be achieved. Porous silicon is a useful material that fouls at slower rates when compared to polymer membranes, and provides a surface which can be easily functionalized [29].

Traditional polymer membranes are insufficient to desalinate hydraulic fracturing flowback water because of high fouling tendencies. Fouling can be caused by numerous factors including formation of a cake layer, blockage of membrane pores, and membrane absorption [30]. Due to the hypersaline composition, intense chemical cleaning of the polymer membranes is required to sustain optimal flux values [31]. However, this cleaning process deteriorates the integrity of the polymer membrane and causes permanent damage. Porous alumina membranes provide another possible option but are limited by pore uniformity and pore size [32]. Porous silicon, however, provides promising anti-fouling properties, such as resistance to chemical corrosion, pore uniformity, and a wide range of possible pore sizes [33, 34, 35]. Additionally, porous silicon can be easily functionalized to form hydrophobic vapor traps [28].

A large portion of this thesis focuses on the development of a porous silicon membrane recipe. Porous silicon is an ideal material for membrane construction, since it has the ability to create a large number of cylindrical pores within a small surface area and is able to withstand the membrane fouling and scaling intrinsic to polymers. Similarly, pore diameter and length can be easily varied. The body of this thesis can be divided into three main chapters:

Chapter 2: Fabrication of porous silicon membranes

This chapter focuses on the development of a porous silicon recipe and the design of an etch cell to contain the anodization reaction. Additionally, characteristics of the produced membranes and post etch modifications will be discussed.

Chapter 3: Forward osmosis testing methodology and design

This chapter focuses on the design and fabrication of a testing station, that will be used to measure the flux. Moreover, the use of dye spectrometry to determine mass changes will be described.

Chapter 4: Forward osmosis results and discussion

This chapter presents the results from the testing of the porous silicon membranes fabricated in the preceding chapters.

Chapter 2

Fabrication of porous silicon membranes

The fabrication of porous silicon is discussed in this chapter, including the design and build of a custom etch cell which contained the anodization electrolyte. Post etch modifications, including the functionalization of the hydrophobic chapter, are also described.

2.1 Porous silicon theory and literature review

A membrane with billions of nanopores is required to effectively test the scalability of desalination using hydrophobic vapor traps. Due to the large number of pores required, nanomachining, and other fabrication methods are not feasible. Porous silicon, however, provides an attractive alternative because of the ability to generate billions of pores though an electrochemical process. Having a silicon substrate base is important because it means that issues with polymer-based membranes fouling and scaling in hyper-saline solutions will likely be mitigated [12].

A large portion of this project was spent developing a porous silicon process sheet, which can be found in Appendix A. Notably, while several recipes for porous silicon have been reported in the past, there is no standard process [33, 34, 35]. The detailed process sheet outlines the methods and specific protocol used to fabricate porous silicon reported in this honors thesis. This recipe has been refined and optimized for the equipment available in Scott Laboratory W489 in the Microsystems and Nanosystems Laboratory.

The fabrication of porous silicon involves working with hydrofluoric acid (HF), which is classified as a contact poison and is rated as a 4 on the NFPA 704 hazardous material standard. This means that extensive research into HF compatible materials, recommended PPE, disposal procedures for incident waste, and contents of the HF first aid kit was completed. Additionally, in Appendix A there is a recommended layout for how these materials and equipment should be organized while completing the anodization etch in the fume hood.

Porous silicon is formed though an anodization reaction. This process requires the use of two electrodes, a HF based electrolyte, an etch cell, a constant current source, an aluminum contact strip, and additional wiring to complete the circuit. Figure 7, contains a schematic of the etch cell and electrical components. For this project, a platinum wire was used as the cathode and, by definition, was responsible for providing electrons to the solution. A silicon wafer was used as the anode, in this case the working electrode, and was responsible for removing electrons from the electrolyte. The etch cell exposes 1.13 cm^2 of silicon wafer to the electrolyte. Thus, in order to limit the reaction at the anode, 5 cm of 18-gauge platinum wire was spiraled into a flat disk. This corresponds to a surface area of 1.6 cm^2, which is greater than the surface area of the anode. This guarantees the reaction is not limited by the amount of electrons the cathode can provide to the solution.

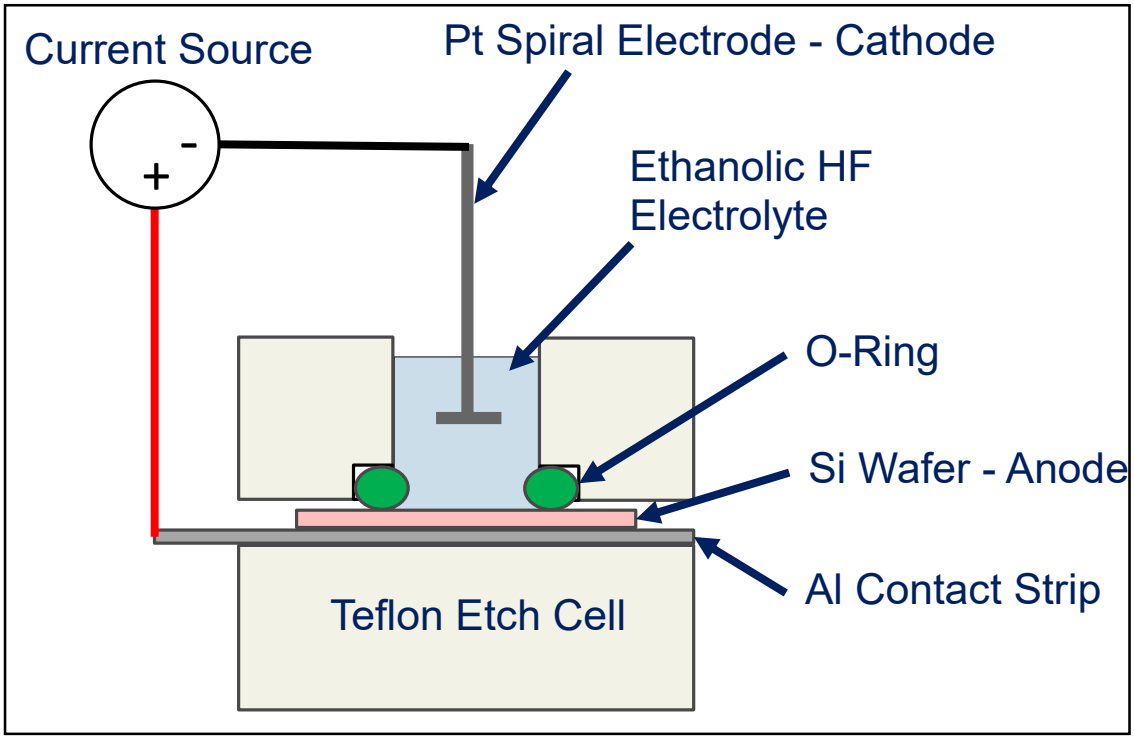

Figure 7: Circuit set-up during anodization etch.

For this project, p-type (boron doped) silicon wafers, purchased from University Wafer, were used as the base substrate. The wafers were degenerately doped with boron to a resistivity of 0.001–0.005 Ω-cm and were single side polished. Wafers doped to this extent are commonly referred to as, p^{++}-type, because of their metallic-like conductivity. Boron p^{++}-type wafers have been shown

to produce a wide variation in pore diameter from 2 nm to 800 nm [35]. This is advantageous because the pore diameter has a direct impact on the efficacy of the hydrophobic vapor traps for desalination. It has been shown that variations in applied current during the anodization etch of p^{++}-type wafer can change the pore diameter, meaning new geometry can be easily tested [33, 34, 35].

The fabrication of porous silicon membranes occurs in two stages. In the first stage the pores are formed in the silicon substrate using a high current density and highly concentrated HF electrolyte. Thus, this stage is referred to as the pore formation etch. In atmospheric conditions silicon spontaneously reacts with oxygen to form a thermodynamically stable silicon dioxide layer. However, during the etch environment, the silicon has access to an abundance of HF. Si-F is the only bond stronger than Si-O, so it is the stronger bond enthalpy which causes the dissolution of the initial oxide layer. In the pore formation etch a 3:1 (v/v) solution of 49% aqueous HF and absolute ethanol was used. A constant current density of 90 mA/cm^2 was applied across the electrode for 5 minutes, using an Agilent E3648A power supply in constant current mode. Thus, for this project a current of 108 mA is required, due to 1.2 cm^2 of the silicon wafer being exposed During this process two half reaction are occurring. Equation 1 occurs at the cathode, and is responsible for reducing the protons to hydrogen gas. This is visible during the experiment because small hydrogen bubbles can be seen on the surface of the electrolyte. These bubbles occur during the electrolysis of water, and can be seen in Figure 8. Equation 2, occurs on the anode and is the primary mechanism for pore formation.

$$\text{Cathode: } 2H^+ + 2e^- \rightarrow H_2 \quad (1)$$

$$\text{Anode: } Si + 6F^{-1} + 2H^+ + h^+ \rightarrow SiF_6^{-2} + H_2 \quad (2)$$

Figure 8: Hydrogen bubbles occurring during the pore formation etch.

In the second stage, the porous silicon portion is removed from the underlying silicon substrate and will be referred to as the detachment etch. The detachment etch requires a 3:46 (v/v) solution of 49% aqueous HF and absolute ethanol. A current density of 3.82 mA/cm^2 is applied for 15 minutes, which corresponds to a total current of 4.5 mA. The low concentration of fluoride ions in the solution forces the reaction on the surface of the silicon to change from producing SiF_6^{2-} to SiO_2. This is significant because a layer of silicon dioxide will form between the porous silicon portion and the silicon base. However, since there is still a small about of fluoride ions in the solution, they will dissolve the recently formed silicon dioxide layer. This will result in a lift off of the porous silicon layer and the creation of a thin membrane. This process can be observed in Figure 9 on the next page.

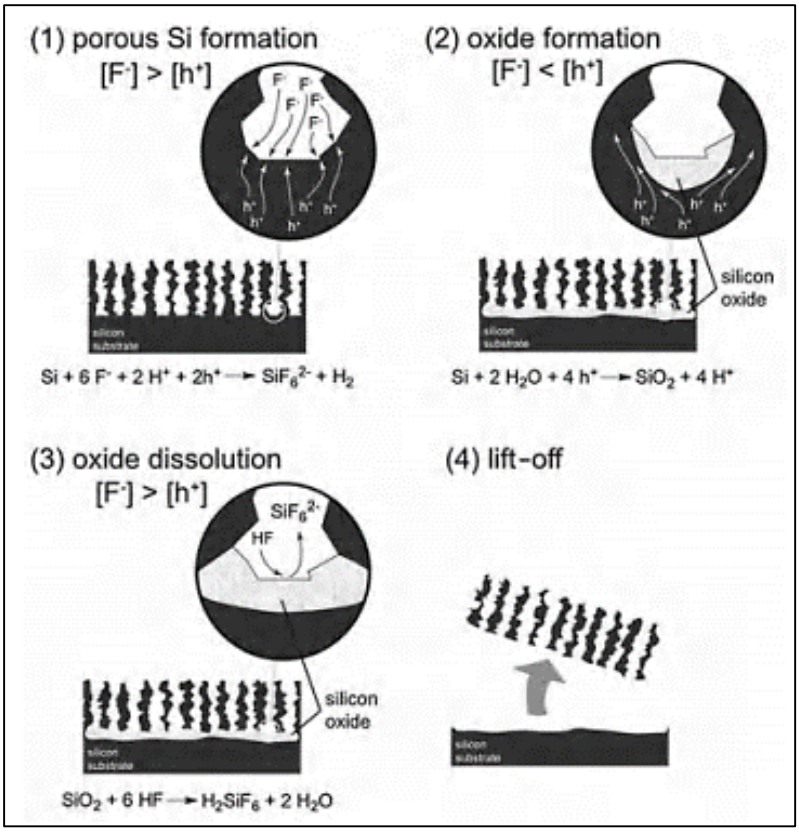

Figure 9: Process that occurs during detachment etch [33].

Once both stages of the etch are complete, the etch cell was thoroughly cleaned to remove access HF and the cell halves were separated to access the membrane. However, sometimes the membrane was still attached to the silicon substrate. This was problematic because the membranes are very brittle and gently pressing on the surface when trying to remove the membrane can cause the membrane to crack. One method that was implemented to ensure detachment was the immersion of the membrane and substrate wafer in a hot water bath at 90 °C. During this process the membrane normally rises to the surface of the bath, while the substrate stays submerges as detailed in Figure 10.

Figure 10: Membrane and substrate placed in water bath to provoke lift-off.

2.2 Development of etch cell

The etch cell was a vital tool used in the fabrication of porous silicon. It is responsible for containing the HF electrolyte and providing a leak-free seal against the silicon substrate. The integrity of the seal must be maintained during the etching process, even when the silicon surface is being modified during the etch. The strength of the bulk material, and resistance to warping, are also crucial to ensuring safety during the etch. For these reasons, Teflon (PTFE) was chose as the etch cell material.

The etch cell is comprised of two parts, a lower half and an upper half. The upper half contains a thru-hole feature which will be used to hold the electrolyte and platinum electrode. There is also an O-ring groove on the underside of the upper half to create the seal. The upper half also has four blind 10 x 24 tapped holes which were used to compress the cell halves, O-ring, and silicon wafer. The lower half contains four thru-holes each with a 10x24 counter bore. Figure 11, contains a rendered image of the final etch cell and a cross section view of the bore that contains the electrolyte. Detailed drawings of the etch cell can be founded in Appendix B.

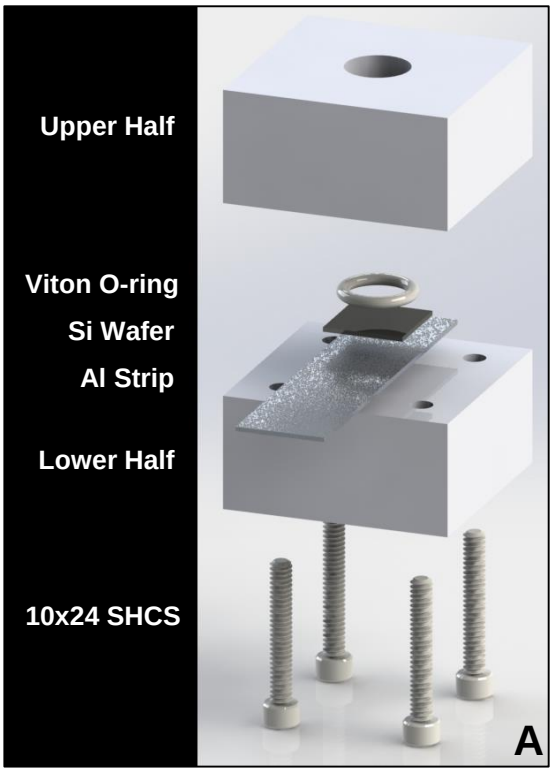

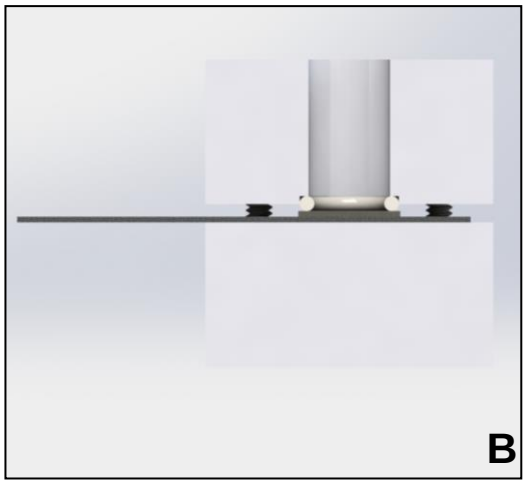

Figure 11: (A) expanded view of etch cell. (B) Cross-section view of thru-hole which contains electrolyte.

Once, the design was finalized, the etch cell was machined in Scott Laboratory W299. No discrepancies from the initial design occurred, and the tolerance of 0.010 inches was maintained. The O-ring groove was machined on a CNC using a number 20 end mill. Figure 12 contains the final, manufactured etch cell. The etch cell is compressed using four socket head cap screws, which ensures adequate O-ring compression. The seal is always tested before each etch by placing ethanol into the cell and inserting a Kimwipe between the surfaces after 5 mins. If the Kimwipe shows signs of wetness, the cell should be taken apart, dried, and compressed again. More details regarding the seal testing process can be found in Appendix A.

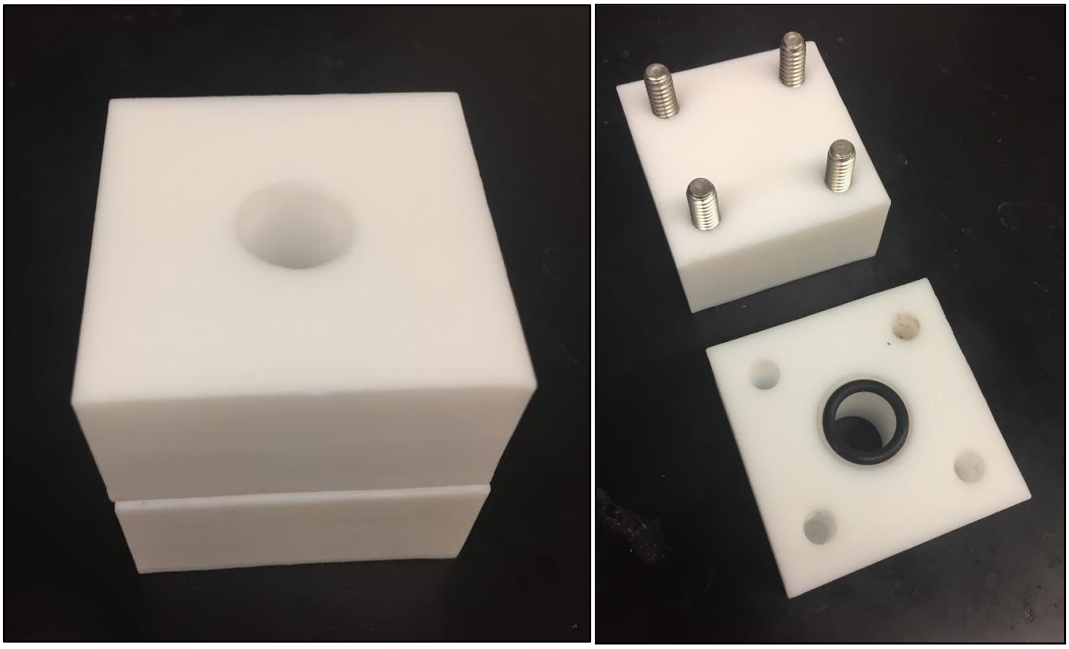

Figure 12: Final etch cell, made of Teflon and machined in Scott Laboratory W299.

2.3 Characterization of porous silicon and SEMs

Adherence to the recipe outlined in Appendix A, will result in a porous silicon membrane with the characteristics outlined in Table 4. Scanning election microscopy (SEM), was performed at the Center for Electron Microscopy and Analysis (CEMAS) to determine the surface structure of the membrane and quality of the pores, as seen in Figure 13. The SEM images were processed and analyzed using ImageJ, in order to more accurately characterize the membrane. Each image was refined using a bandpass filter, which filtered structures smaller the 2 pixels and larger than 40 pixels (each pixel is 3.2 nm). The brightness threshold was then set to 57.7% and the 'analyze particles' function was executed. The image after the bandpass filter and threshold setting can be seen in Figure 14. A magnified image after the 'analyze particles' function can be seen in Figure 15. The resulting data was output to excel and the characteristics of each pore were calculated.

The most significant characteristics outlined in Table 4 are the average pore diameter, which was determined to be 10 ± 2.2 nm, and the pore surface area density, which was calculated to be 23.05%. The pore surface area density is the ratio of total pore area to total membrane area. The

number of pores for the whole membrane was extrapolated from the ImageJ data and was determined to be ~400 billion. This corresponds to ~333 billion pores/cm^2. Pore diameter and surface density are important factors that directly affect the flux and permeability of the membrane. Additionally, a collection of membranes can be seen in Figure 16, where they are compared to a US dime which has a diameter of 1.79 cm.

Table 4: Pore characteristics

Pore Diameter	10 ± 2.2 nm
Surface Pore Density	23.05%
Thickness	10 ± 1.3 μm
Membrane Area	1.2 ± 0.2 cm^2
Pores per Membrane (estimated)	300-500 Billion

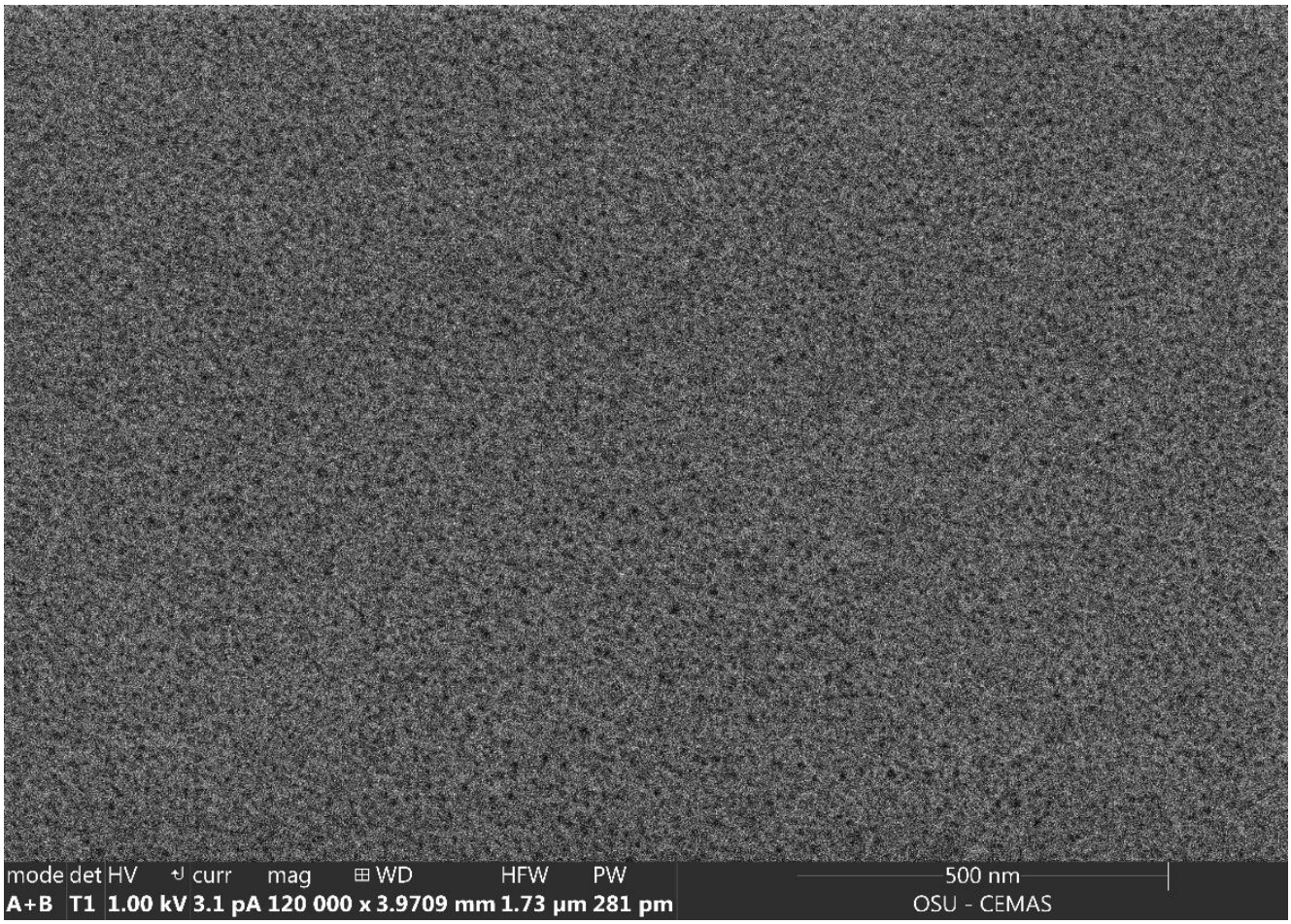

Figure 13: SEM images used to determine membrane characteristics.

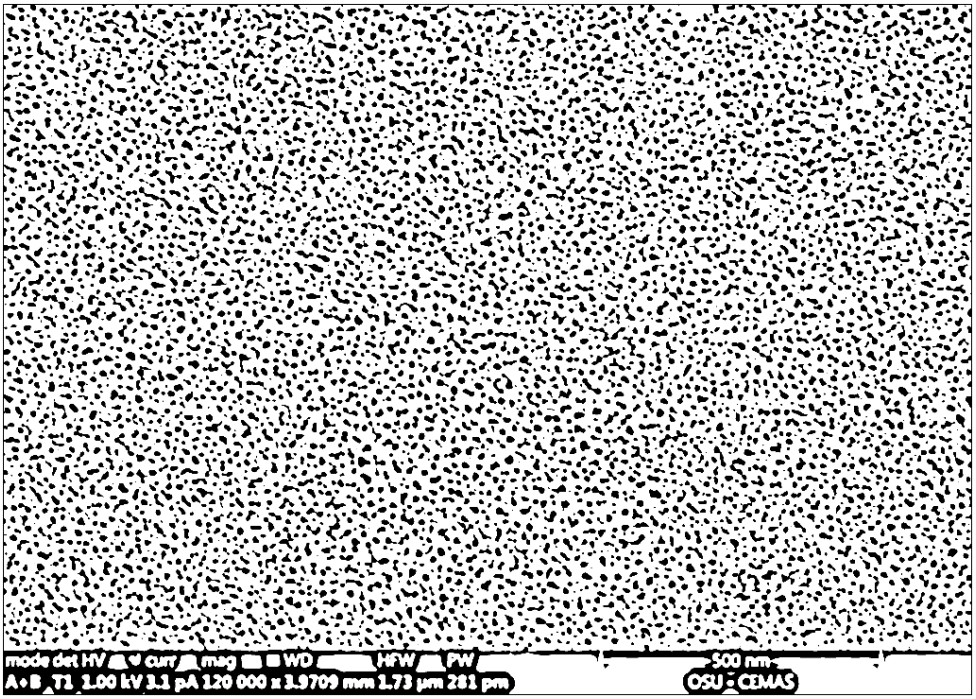

Figure 14: SEM image after bandpass and brightness threshold adjustment in ImageJ.

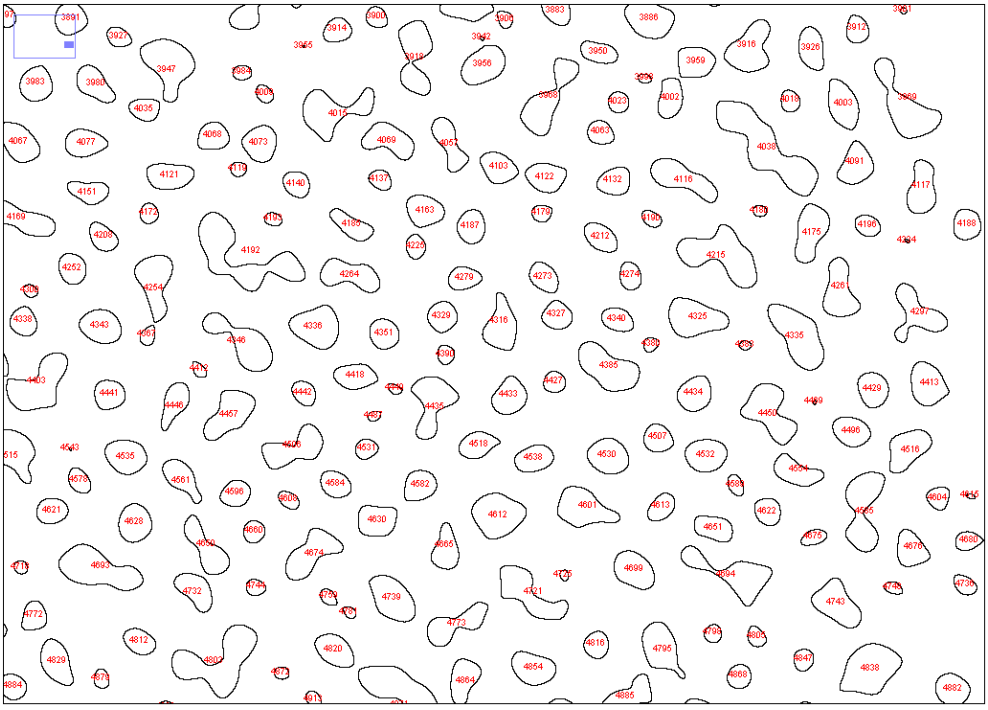

Figure 15: SEM image after performing ‘analyze particles’ function in ImageJ.

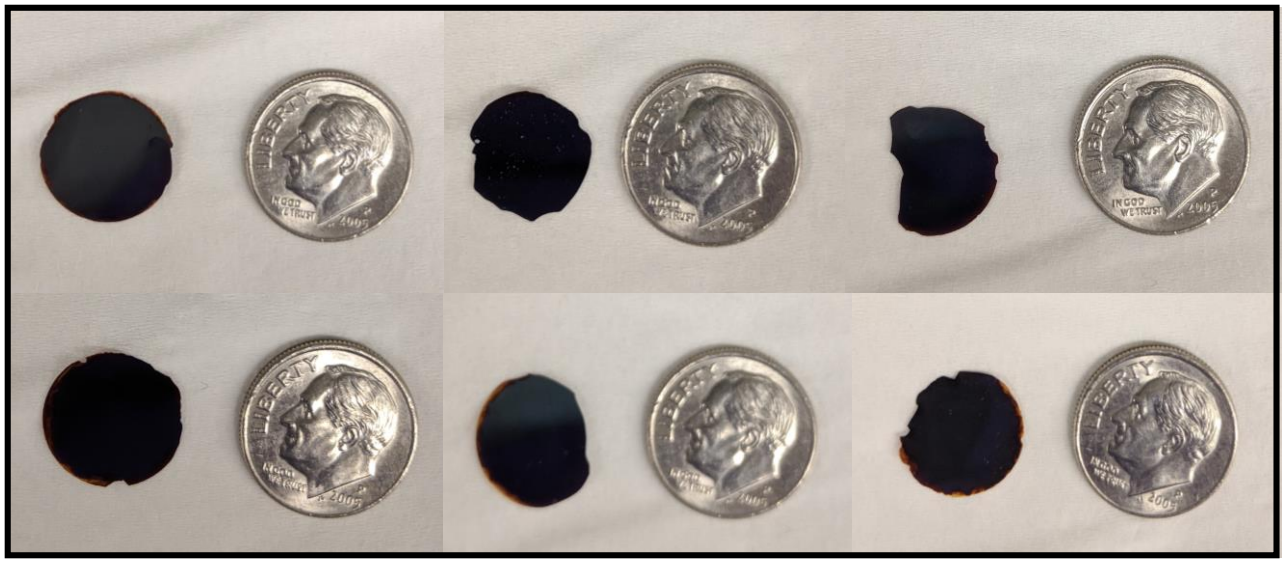

Figure 16: Sample porous silicon membranes.

2.4 Membrane support for permeation tests

As explained above, the porous silicon membranes fabricated during this project are very brittle. This is problematic because even gently handling the membranes can result in a crack. In order to make the membranes easier to handle and able to withstand the stresses which occur during testing, the outer edge of the membranes must be supported.

For this project a nylon washer with a 0.875 in outer diameter and a 0.344 in inner diameter was used. The membrane was placed polished side down on the surface of the washer, and a line of Double Bubble Orange epoxy was place on the outer edge of the membrane. The epoxy bonds the membrane to the washer and creates a water-tight seal. Figure 17 displays the membranes epoxied to the washer. It is worth noting that before this washer and epoxy combination was determined, other washers and adhesives were also tested. Zinc O-rings were tested but were unable to bond with the Double Bubble Orange epoxy. Additionally, Weld-On 16 was used as a possible adhesive choice, but during the curing process, it was observed that the membranes would crack.

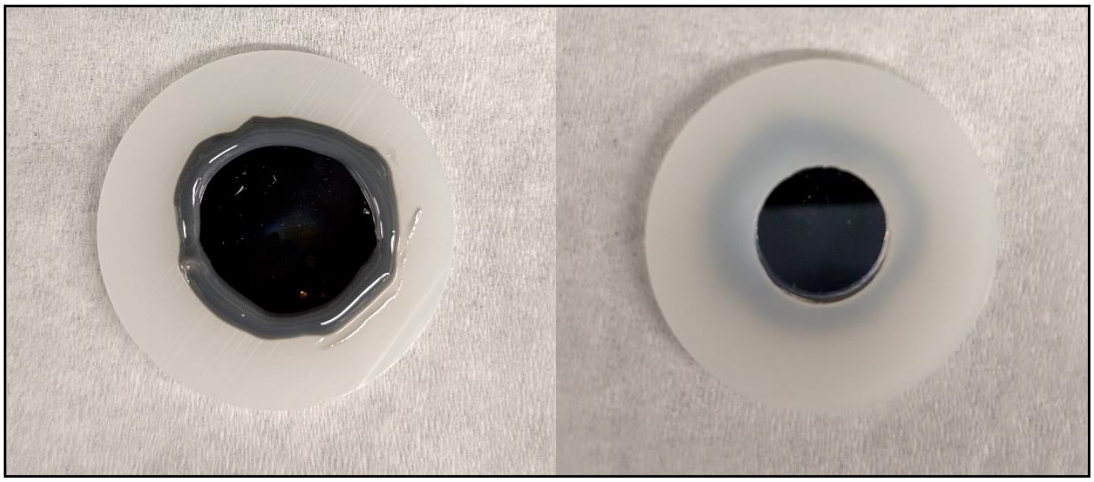

Figure 17: Porous silicon membrane epoxied to nylon washer.

2.5 Functionalization and contact angle measurements

Creating hydrophobic pores is crucial to obtaining the osmotic vapor pressure gradient. This process is referred to as functionalization and is completed by depositing a silane layer on the pore walls. For functionalization, the porous silicon membranes were immersed in a 0.5% (v/v) Octadecyltrichlorosilane (OTS) and 100% anhydrous toluene bath for one hour. This process occurred in a nitrogen gas dry bag, in order to decrease the volatility of the silane.

The functionalization of the membrane was confirmed through contact angle measurements on a Rame-Hart goniometer, located in Scott Laboratory W489. A water droplet of 20 μl was placed on both sides of a functionalized and non-functionalized wafer. It was determined that for non-functionalized membranes the average contact angle was 70.8º. This is expected because silicon is naturally hydrophilic and hence a contact angle less than 90º is expected. It was also determined that the functionalized membrane had a contact angle of 106.2º. Measurements were taken on both side of the membrane in order to ensure full functionalization of the membrane. Figure 18 contains images that were used to calculate the contact angle.

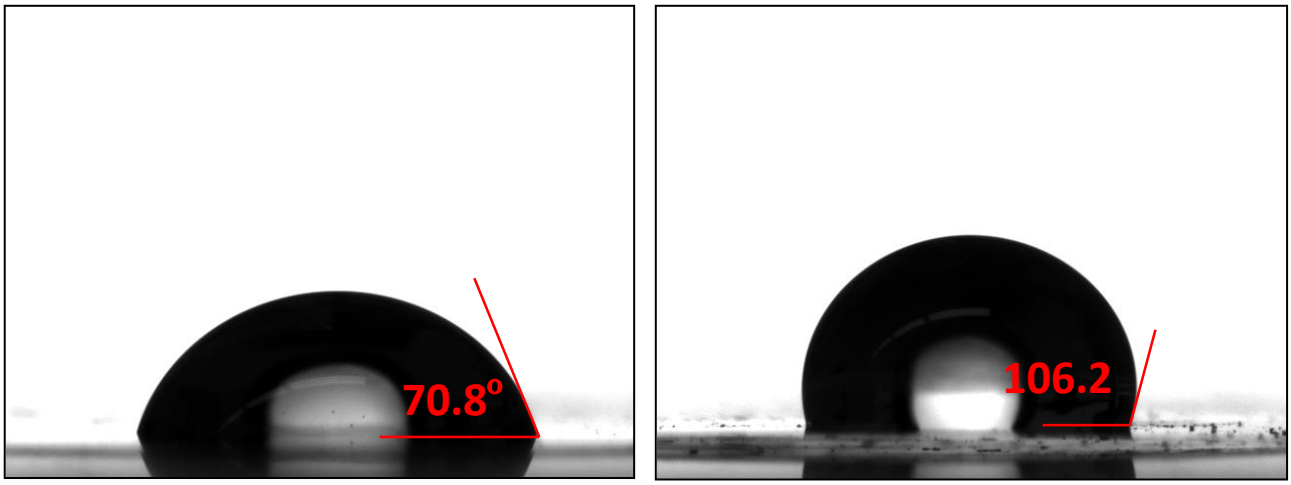

Figure 18: Sample porous silicon membranes.

Chapter 3

Forward osmosis testing methodology and design

This chapter focuses on the design of the testing system that will be used to measure flux across the membrane. Various iterations of the testing station will be discussed as well as the how the spectrometer was used to measure changes in concentration.

3.1 Design of testing station

Once the porous silicon membranes were fabricated the next goal was to test for the permeation across these membranes. Therefore, the immediate task was to design and build a testing station. The testing station was comprised of two cells that are separated by the membrane and a sealing mechanism. Appendix C includes the detailed drawings for the testing station. The cell walls were constructed from 0.25 in thick acrylic sheet. The sheet was laser cut into the required parts and then the parts were bonded together using Weld-On 16. Prior to reinforcing the membrane with a nylon washer, the seal was going to be created by Viton rubber gaskets. However, it was determined that these gaskets were unable to create a leak-free seal without excessive compression which usually cracked or broke the membranes. Thus, the washer reinforcement was implemented and sized with available surface on the outer edge of the washer to compress an O-ring against. This enables a leak-free seal to be created with O-rings, while concentrating the compression stresses in the body of the washer. Additionally, each cell half contains an O-ring groove and 0.5 in thru-hole. The 0.5 in thru-hole was designed to be larger than the washer's 0.344 in inner diameter, in order to ensure the exposed area of the membrane is the limiting area. The cells were then compressed using four 10 x 24 socket head cap screws. One side of the testing station contains the required 10 x 24 tapped holes. Figure 19 contains a rendered, expanded-view of the design.

Fabrication of the testing station was completed in Scott Laboratory W299. The walls of the testing station were laser cut in Scott Laboratory W170 and were adjust by 0.5 mm on all dimensions to account for the focal point of the laser. The O-ring, tapped hole, and bonding was completed in W269. There were no deviations from the final design during construction, and the tolerance of 0.010 inches was maintained. The final testing station can be seen in Figure 20.

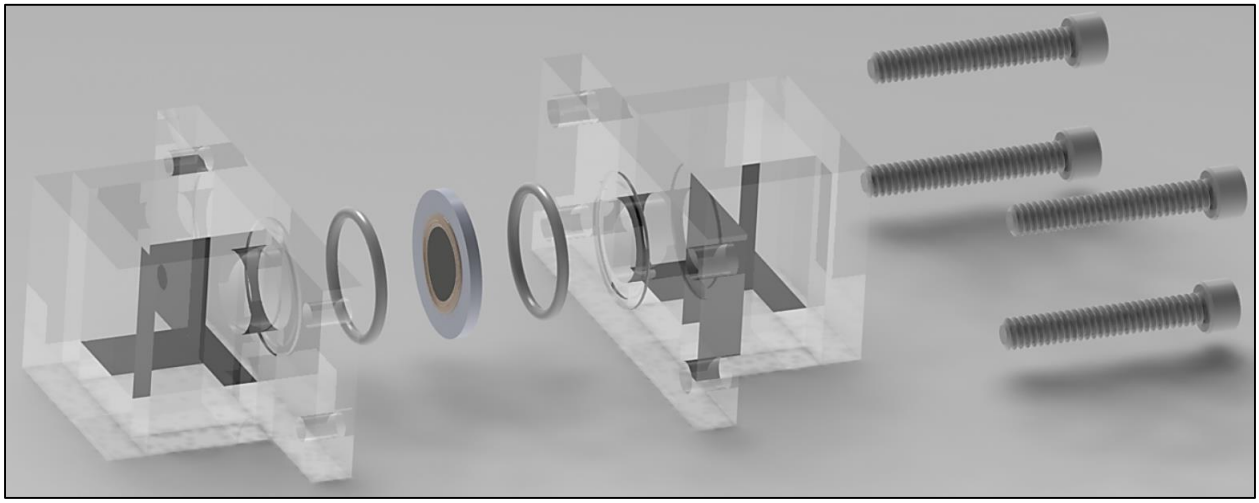

Figure 19: Exploded view of designed testing station.

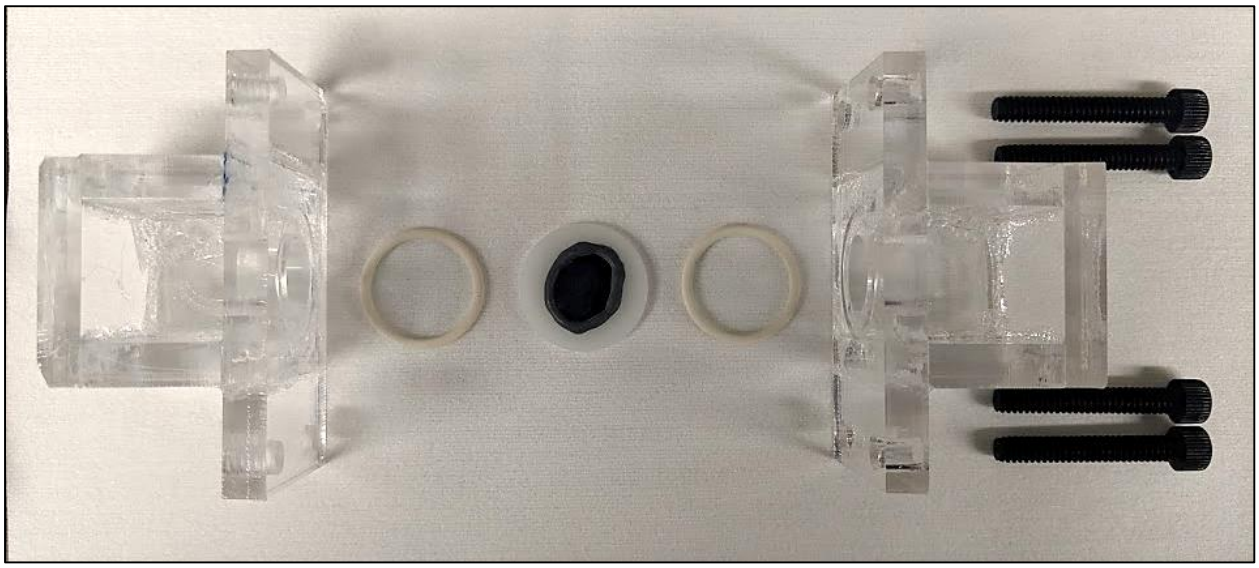

Figure 20: Actual testing station fabricated in W269

3.2 Spectrophotometer to measure concentration

The change in concentration of the draw and feed solutions was determined by measuring the absorption of methylene blue dye used as a marker for transport across the porous silicon membranes. The draw solution was 100 mM of sodium chloride with 0.05 mM of methylene blue. The feed solution was DI water. The absorption spectrum of methylene blue was measured, and the absorption peak was observed at 664 nm in accordance with past results [36]. Then a calibration curve of absorption and methylene blue concentration was developed with a fit line. The calibration curve is seen in Figure 21. Since the relationship between methylene blue absorption and concentration is now known, as the draw dye desalts, the exact salt concertation can be calculated.

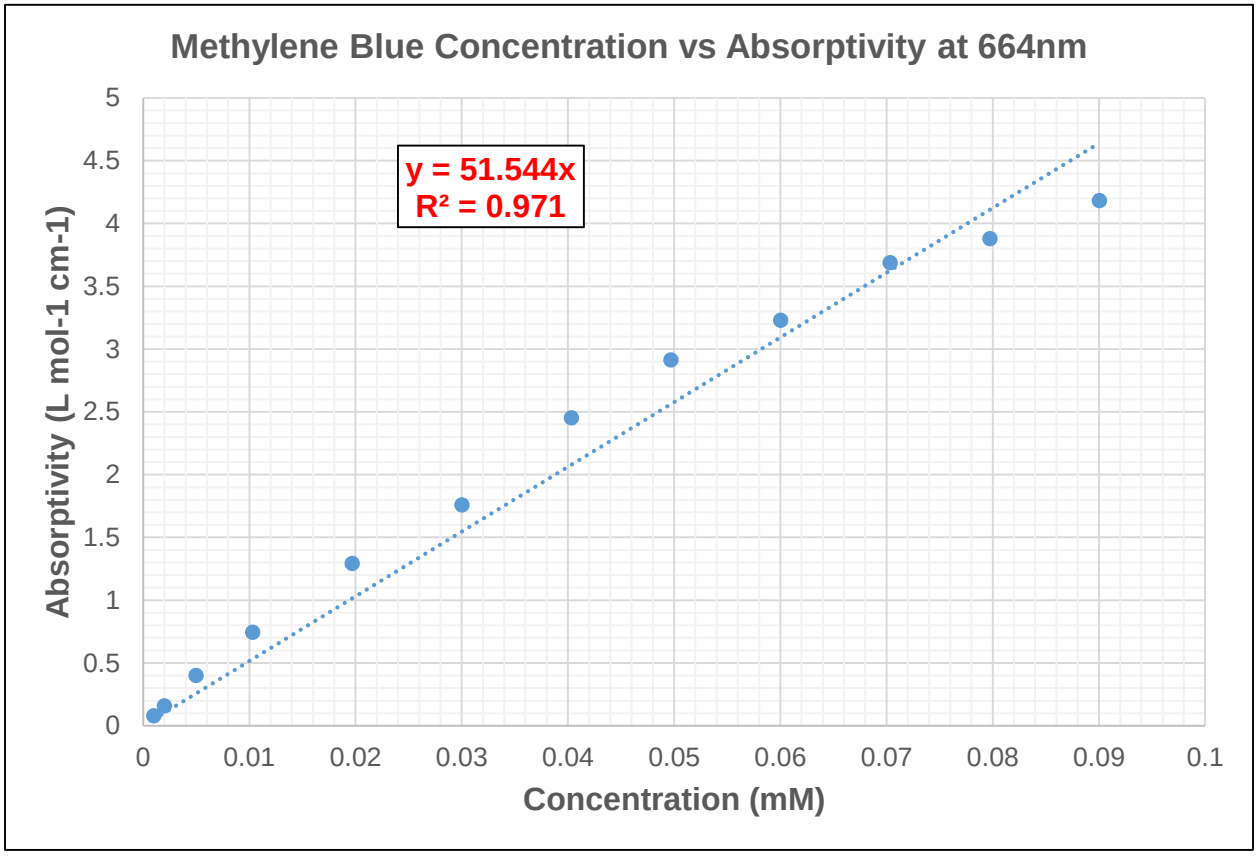

Figure 21: Methylene blue concentration and absorption calibration curve.

The instrument settings and calibration data for the UV-Vis spectrophotometer are show in Appendix D. It is worth noting that the baseline measurement for the spectrometer was the absorbance of an empty cuvette.

3.3 Testing set-up

During the testing process, 9 mL of draw and 9mL of feed solution are place in their respective testing cell sides. During all experiments, the polished side of the silicon wafer was placed on the draw solution side. Similarly, the epoxied side of the membrane was always placed on the feed solution side. The cells were compressed and the forward osmosis experiment was conducted for 24 hours. During the testing process, a piece of Parafilm was placed over the testing station in order to reduce evaporation.

Once the forward osmosis experiment was completed, the solution on each side was removed and the volume was recorded. Then the absorbance of each side was measured and a concentration was calculated using the linear fit. Figure 22 displays the visible change in concentration that is apparent after 24 hours.

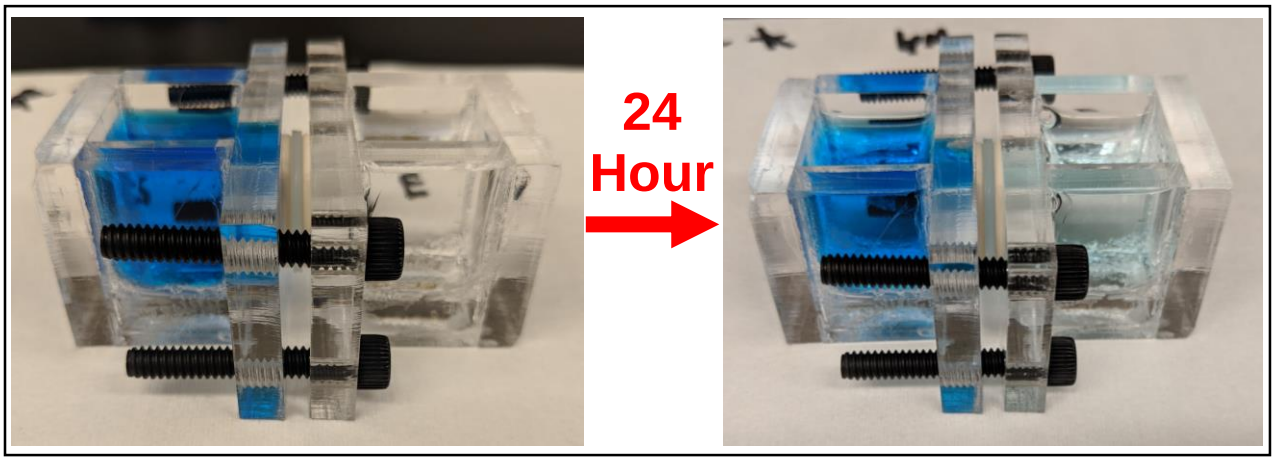

Figure 22: Noticeable concentration change in draw and feed solutions after 24 hours. The membrane tested in this photo was non-functionalized.

Chapter 4

Forward osmosis results and discussion

This chapter explains the outcome of each membrane, and presents the results from the forward osmosis testing. The desalting capabilities of functionalized and non-functionalize membranes are compared. Additionally, inspection of membranes after testing are discussed.

4.1 Outcome of each etch

Throughout this project, 36 etches were completed. The outcome of each etch can be seen in Figure 23. A complete logbook of each etch is attached in Appendix E. At the beginning of the project, four etched were completed with spare, 0.31Ω-cm wafers. This was to practice and refine the etching process so no careless errors were made with the 0.001–0.005 Ω-cm wafers.

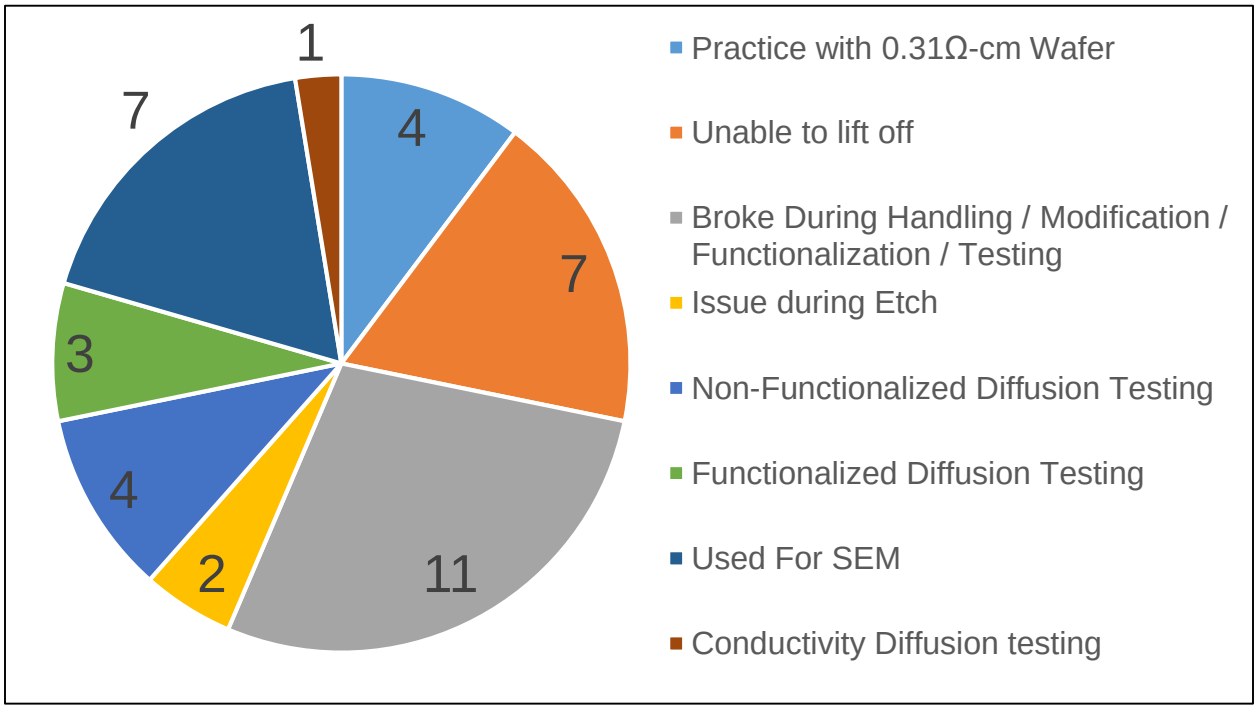

Figure 23: Outcome of 36 etches.

Furthermore, before implementing the water bath to initiate lift-off, seven membranes were damaged trying to remove the porous section from the underlying substrate. Additionally, eleven

membranes were broken during post etch modification, excessive compression during testing, and mishandling. The end result was 7 total membranes were available for permeation testing.

4.2 NaCl draw results and discussion

Four, non-functionalized membranes each underwent two, 24-hour forward osmosis experiments. DI water was used as the feed solution, and 100 mM NaCl with 0.05 mM of methylene blue was used as the draw solution. Using these solutions, the osmotic pressure experienced by the membrane was calculated using equation 3 to be Π = 4.83 atm. It is worth noting that in this equation, i represents the van't Hoff factor which is the number of ions which have dissociated from the initial solute. Additionally, all forward osmosis tests were performed at room temperature, T = 294 K. At the start of the forward osmosis test, 9 mL of the draw and feed solutions were placed into their respective sides of the testing station. The testing station was then covered with a piece of Parafilm to minimize evaporation. For similarity, the draw side of the solution was always placed in contact with the polished side of the membrane. Using non-functionalized membranes allow a baseline desalting rate to be calculated and compared to the functionalized membranes, which are expected to be higher.

$$\Pi = MRTi \tag{3}$$

$$\Pi = (100mM)(0.08296\ \frac{l * atm}{mol * K})(294K)(2)$$

$$\Pi = 4.825\ atm$$

Over a 24-hour period, the average desalting of the draw solution was calculated to be 24.25% for a non-functionalized membrane. Once the forward osmosis period was complete, the volume of each side was removed and measured. It was determined over the 24-hour period that 2.22% of the initial volume was lost. This loss is minimal and can be attributed to fluid remaining on the sides of the cell, fluid still contained inside the pores of the membrane, and fluid that had evaporated. Additionally, the average percentage of methylene blue moles lost was also calculated

to be 14.92%. This is quite high but could can be attributed to absorption of the dye by the O-rings, which can be seen in Figure 24.

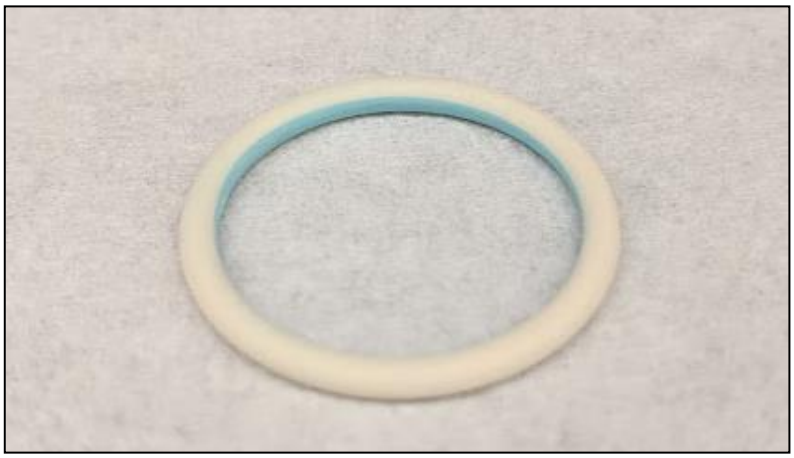

Figure 24: Methylene blue dye absorber by O-ring

Identical forward osmosis experiments were performed on three functionalized membranes. The average desalting was calculated to be 2.43% During these experiments the average percent volume lost was 2.22% and the percent of methylene blue moles lost was 1.81%. A comparison of the non-functionalized and functionalized membranes can be seen in Table 5. Forward osmosis calculations are attached in Appendix F.

Table 5: Comparing the desalting ability of functionalized and non-functionalized membranes.

Membrane Type	Average Draw Dilution (%)	Number of Membranes	Number of Tests
Non-Functionalized	24.25	4	8
Functionalized	2.22	3	6

What is interesting about these results is that it was hypothesized the non-functionalized membranes would have a higher desalting ability, as evidenced by the Nano-scale experiments [28]. However, this was not the case in the porous silicon membranes, which had minimal water transport. It is likely this discrepancy is occurring due to a number of reasons including: the length of the hydrophobic portion, pore diameter, and issues with the methylene blue absorption-concentration process. Additionally, it is worth noting that the desalting ability of non-functionalized membranes varies based on if the membrane had already been tested. As explained,

each membrane was tested twice, once when new and once when reused. When these results are compared the average desalting of the reused membrane decreased by 2.24%. This can be observed in Table 6.

Table 6: Comparison of desalting ability before and after use for non-functionalized membranes.

Membrane Type	Average Draw Dilution (%)	Number of Membranes	Number of Tests
Non-Functionalized New	25.34	3	3
Functionalized After 1 Use	23.1	3	3

In order to understand the impact of exposing the membrane to the brine draw solution, an SEM image of a tested membrane was taken and can be seen in Figure 25. It can be observed that the pores may be collapsing during the testing process and forming larger pores with more combined structures observed. This is evidenced by the lack of uniform 10 nm pores that were present in Figure 13, and the appearance of larger, rougher shaped pores. It is predicted that stresses which occur during the evaporation of liquid in the pores is risible for pore collapse. The capillary stresses due to surface tension have been determined to reach stress of up to 6 MPa [37, 38]

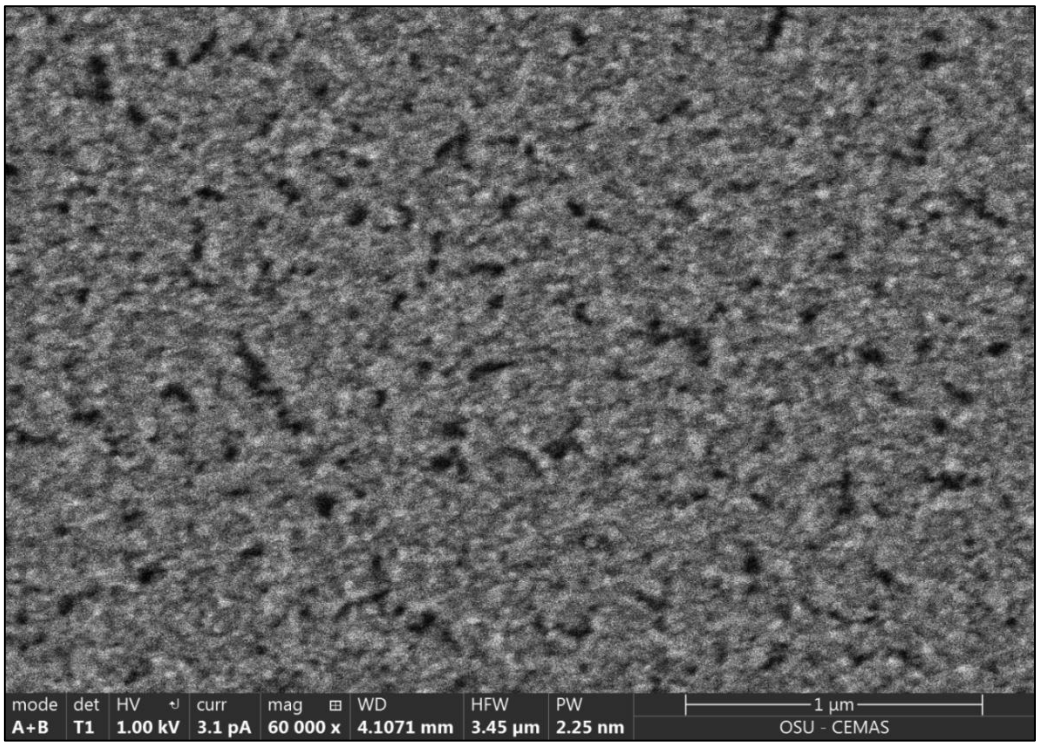

Figure 25: SEM image of non-functionalized membrane after one forward osmosis test.

Chapter 5
Conclusions and future work

This chapter summarizes the importance of localized energy independence and outlines the need for a cost-effective hydraulic fracturing flowback desalter. The progress creating porous silicon membranes is discussed and initial forward osmosis results are explained. Future work to minimize pore collapse during testing is also discussed.

5.1 Conclusions

This project outlines the successful fabrication of a porous silicon membrane, which can be used to scale-up nanochannel desalination experiments. These nanochannel experiments were able to utilize hydrophobic vapor traps and desalt a draw solution by 95% every 20 minutes. First, a porous silicon recipe was developed and the required etch cell used to contain the electrolyte was fabricated. The resulting porous silicon membranes have an average pore diameter of 10 ± 2.2 nm and a surface density of 23.05%. Then, the post-etch procedures for functionalizing and reinforcing the membrane were created and implemented. The testing apparatus was also fabricated and used to measure flux across the membrane.

It was determined the non-functionalized membranes have an average desalting capacity of 24.25% during a 24-hour period. This project was able to create a test procedure that can work for any future membranes produced.

5.2 Future work

To more accurately characterize the fabrication process and water transport process through the membrane, it would be beneficial to obtain cross-sectional SEM images of the membrane. This would determine if the pores are completely cylindrical or are tapered. Additionally, if cross-sectional SEM images are taken before and after forward osmosis testing, for both non-functionalized and functionalized membranes, the desalting rates can be more clearly understood.

For future experiments it is recommended to transition to a conductivity-based measurement system, to determine concentration of the feed and draw solutions. Instead of measuring absorbance, the conductivity of the solutions could be measured to get a direct TDS reading. This would reduce measurement time and error induced by the methylene blue. Methylene blue is a positively charged molecule and its interaction with OTS silane at the porous silicon interface is unknown [39]. Preliminary measurements have been explored using the conductivity method, but the volume of each testing cell is not large enough to submerge the conductivity sensor. Thus, controlled dilution is required to increase the volume of each side.

Additionally, the functionalization process should also be refined to obtain higher contact angle readings. It is unknown whether there is an OTS silane monolayer along the interior surface of the pores. It is recommended that future membranes are submerged in the OTS silane and toluene solution for more than 1 hour. An increase in time may increase the efficacy of the functionalization and result in a higher contact angle.

Another area of focus would be to optimize characteristics of the membrane. Table 7 compares the cross-section and length of the pores used in this project, with the dimensions of the nanochannels used in the proof of concept. Issues with the pores collapsing due to evaporation stresses could be remedied by modifying the pore diameter and thickness of the membrane. Pore diameter can be varied by increasing the current density during the pore formation etch. It is important to carefully observe the electrolyte during higher current densities because more bubbling is likely. Additionally, the thickness of the membrane can be increased by lengthening the duration of the pore formation etch.

Table 7: Comparison of porous silicon pores and proof-of-concept nanochannels.

	Porous Silicon	**Nanochannel**
Pore Cross-section	10nm Diameter	30μm X 80nm
Hydrophobic Length	10μm	96μm and 480μm

Bibliography

[1] U.S. Energy Information Administration, “April 2018 Monthly Energy Review,” Table 1.4, pp.10, 2018.

[2] Boersma, T., et al., “U.S. Energy Diplomacy,” *Columbia Center on Global Energy Policy*, February, 2018.

[3] Faramawy, S., “Natural gas origin, composition, and processing: A review,” *Journal of Natural Gas Science and Engineering*, vol. 34, pp. 34-54, 2016.

[4] ODNR Division of Oil & Gas Resources, *Oil and Gas Well Production* [Online]. Available: http://oilandgas.ohiodnr.gov/

[5] Soeder, D.J., “The Marcellus Shale: Resources and Reservations,” *EOS, Transactions, American Geophysical Union*, vol. 91, pp. 277- 288, 2010.

[6] U.S. Energy Information Administration, “Frequently Asked Questions,” [Online]. Available: https://www.eia.gov/tools/faqs/faq.php?id=50&t=8

[7] Rahm, Dianne, “Regulating hydraulic fracturing in shale gas plays: The case of Texas,” *Energy Policy*, vol. 39, pp. 2974-2981, 2011.

[8] Prakash, S., Bellman, K., Challenges and Opportunities for Nanotechnology in the Energy Water Nexus. In AquaNanotechnology, Editors: D.E. Reisner and T. Pradeep, CRC Press, 2014, 563-586

[9] Gregory, K. et al., “Water Management Challenges Associated with the Production of Shale Gas by Hydraulic Fracturing,” *Elements*, vol. 7, pp. 181-186, 2011.

[10] Kondash, A. et al., “Quantity of flowback and produced waters from unconventional oil and gas exploration,” *Science of the Total Environment*, vol. 574, pp. 314-321, 2017.

[11] *What is Hydraulic Fracking?*, H2O Distributers [Online]. Available: https://www.h2odistributors.com/pages/contaminants/contaminant-fracking.asp

[12] Shaffer, D. L., et al., “Desalination and Reuse of High-Salinity Shale Gas Produced Water: Drivers, Technologies, and Future Directions,” *Environmental Science & Technology*, vol. 47, pp. 9569-9583, 2013.

[13] Greenlee, L. F., et al., “Reverse osmosis desalination: water sources, technology, and today's challenges,” *Water Research*, vol. 43, pp. 2317-2348, 2009.

[14] Fritzmann, C., et al., “State-of-the-art of reverse osmosis desalination,” *Desalination*, vol. 216, pp. 1-76, 2007.

[15] Bakken Smart, “Water Fact Sheet,” [Online]. Available: https://www.undeerc.org/bakken/pdfs/NDIC-NDPC-Water-Fact-Sheet.pdf

[16] Environmental Protection Agency, “Proceedings of the Technical Workshops for the Hydraulic Fracturing Study: Water Resources Management,” May 2011.

[17] Ellsworth, W.L., et al., “Injection-Induced Earthquakes,” *Science*, vol. 314, 2013.

[18] Auch, T., *Ohio Shale Oil and Gas Viewer*, Fracktracker Alliance [Online]. Available: https://www.arcgis.com/home/webmap/viewer.html?useExisting=1

[19] USGS, “Estimated Use of Water in the United States in 2015,” *Water Availability and Use Science Program*, 2015.

[20] Scott, C. et al., “Policy and institutional dimensions of the water–energy nexus,” *Energy Policy*, vol. 39, pp. 6622-6630, 2011.

[21] U.S. Energy Information Administration, “Arizona State Profile,” [Online]. Available: https://www.eia.gov/state/?sid=AZ

[22] Mishra, Pallavi & Soni, Rajshri. “Analysis of Dyeing and Printing Waste Water of Balotara Textile Industries,” *International Journal of Chemical Sciences*, vol. 14, pp.1915-1924, 2016.

[23] Maruf, M. et al., “Removal of TDS and BOD from Synthetic Industrial Wastewater via Adsorption,” *IPCBEE*, vol. 41, pp.166-170, 2012.

[24] Belkin, S. et al., “Biological Treatment of a High Salinity Chemical Industrial Wastewater,” *Water Science and Technology*, vol. 27, pp.105-112, 1993.

[25] Shi, X. et al., “Sequential anaerobic–aerobic treatment of pharmaceutical wastewater with high salinity,” *Bioresource Technology*, vol. 153, pp.79-86, 2014.

[26] Lech, M. et al., “Monitoring of total dissolved solids on agricultural lands using electrical conductivity measurements,” *Bioresource Technology*, vol. 153, pp.79-86, 2014.

[27] Tow, E. et al., “Comparison of fouling propensity between reverse osmosis, forward osmosis, and membrane distillation,” *Journal of Membrane Science*, vol. 556, pp. 352-364, 2018.

[28] Rangharajan, K. K., et al., “Surface dependent enhancement in water vapor permeation through nanochannels,” *Analyst*, vol. 143, pp. 4256-4266, 2018.

[29] Warkiani, M.E., et al., “Isoporous Micro/Nanoengineered Membranes,” *ACS Nano*, vol. 7, pp. 1882-1904, 2013.

[30] Maguire-Boyle, S. et al., “A new functionalization strategy for oil/water separation membranes,” *Journal of Membrane Science*, vol. 382, pp.107-115, 2011.

[31] Miller, D. et al., “Fouling-resistant membranes for the treatment of flowback water from hydraulic shale fracturing: A pilot study,” *Journal of Membrane Science*, vol. 437, pp.265-275, 2013.

[32] Desai, T. et al., “Nanoporous anti-fouling silicon membranes for biosensor applications,” *Biosensors and Bioelectronics*, vol. 15, pp.453-462, 2000.

[33] Sailor, M.J., *Porous Silicon in Practice*, Wiley-VCH: Weinheim, Germany, 2012.

[34] Canham, Leigh, *Handbook of Porous Silicon*, Springer International Publishing: Switzerland, 2014.

[35] Janshoff, Andreas, et al., “Macroporous p-Type Silicon Fabry-Perot Layers. Fabrication, Characterization, and Applications in Biosensing,” *Journal of The American Chemical Society*, vol. 120, pp. 12108-12116, 1998.

[36] Omata, Takahisa, et al., “Photodegradation of Methylene Blue Aqueous Solution Sensitized by Pyrochlore-Related k-CeZrO4 Oxide Powder,” *Materials Transactions*, vol. 44, pp. 1620-1623, 2003.

[37] Pavesi, L., *Silicon Nanocrystals*, Wiley-VCH: Weinheim, Germany, 2009.

[38] Bisi,O., et al., “Porous silicon: a quantum sponge structure for silicon based optoelectronics,” *Surface Science Reports*, vol. 38, pp. 1-126, 2000.

[39] U.S. National Library of Medicine, “ Methlyene Blue Compound Summary,” *PubChem*, [Online]. Available: https://pubchem.ncbi.nlm.nih.gov/compound/methylene_blue

Appendix A

Porous silicon process sheet

Process sheet for fabricating mesoporous silicon film (thickness: 10µm, pore diameter: 10nm)

Abbreviations

PS (Porous Silicon), IPA (Isopropyl Alcohol), PP (Polypropylene), PE (Polyethylene)

Materials

- Pt spiral electrode (1mm dia. with spiraled portion equivalent to 4.5cm unraveled)
- Al contact strip (2cm x 6cm)
- Silicon wafer; P^{++}-type, B-doped, SSP, (100), resistivity <0.005 ohm-cm
- Etching electrolyte (See note 1 for preparation)
- Detachment electrolyte (See note 2 for preparation)
- Ethanol (200 proof)
- Isopropanol
- Cyclohexane

Equipment

- PE pipets
- PE bottles with spout (to rinse equipment)
- PP 30mL beakers
- Pyrex 250mL beaker
- HF resistant enclosure (Carboy container cut in half)
- Incidental HF rinse bucket (PP jug cut in half)
- HF incident waste container
- HF waste container
- Solvent waste container
- HF resistant tweezers
- Agilent power supply
- Banana to alligator clips (1 x red, 1 x black)
- Air gun
- Diamond tipped scribe
- Straight edge
- Support stand with clamp
- Kim-wipes
- Para film

- Tape
- Ultrasonic bath
- Teflon Etch Cell
- Black Sharpie Marker
- Paper

PPE

- Face shield
- Safety glasses
- Rubber apron
- Nitrile gloves
- Neoprene gloves
- Fume hood
- HF first aid kit

Process

Label and Position Equipment in the Fume Hood

1. *Steps 2-10 do NOT require any PPE.*
2. Consult Figure 1 and Figure 2, located on the final page, for details regarding the location of equipment in the fume hood.
3. Position the HF acid waste container, HF incidental waste container, ethanol waste container, and physical waste bin close to the fume hood. Ensure the physical waste bin is open.
4. Position the power supply on the left side and use the electrical socket on the outer left side of the fume hood. Plug the banana connectors into the correct ports on the power supply (negative – black, positive – red).
5. To the right of the power supply, position the HF resistant enclosure.
6. Place the support stand behind the HF resistant enclosure, and attach the clamp to the support so it hangs over the enclosure.
7. Place the Pt wire in the clamp.
8. Place the incidental HF rinse bucket to the right of the HF resistant enclosure.
9. Use a black sharpie marker to create paper labels for the beakers, bottles, graduated cylinders, and pipets as outlined in Figure 1. Place the paper labels in their respective locations.
10. Use a black sharpie marker to then label the beakers, bottles, and pipets. Place the containers on top of their labels in the fume hood.

Sizing and Cleaning the silicon wafer

1. *Steps 2-11 require only nitrile gloves and can occur outside the fume hood.*
2. Place the wafer on a Kim-wipe with the polished side facing down.
3. Place a straight edge on the wafer, perpendicular to the primary flat edge.

4. Position the straight edge so a strip approximately 18mm wide is visible.
5. Score the wafer multiple times along the straight edge using the diamond tipped scribe.
6. Once scored, place the wafer polished side up on a pile of Kim-wipes. Apply light pressure to the wafer above the location of the score line. The wafer will break along the score line.
7. Repeat steps 2-6 to cleave the wafer again to produce a 18mm x 18mm square wafer.
8. Place the wafer in a 250mL Pyrex beaker with 20mL of IPA and then place the beaker in the ultrasonic bath for 15 minutes.
9. Remove the beaker from the ultrasonic bath and then use tweezers to place the wafer on a Kim-wipe.
10. Dispose of the IPA in the **solvent waste** container.
11. Dry the wafer with the air gun.
12. *Steps 13-26 occur in the fume hood with appropriate PPE.*
13. **Handling HF is particularly hazardous and thus requires extensive safety precautions. Before working with HF, notify a coworker and instruct them to routinely check on you. Post a sign on the lab door when HF is being used. Wear long sleeved clothing and closed toe shoes. Wear a rubber apron, safety glasses, and face shield. Additionally, wear nitrile gloves inside neoprene gloves which cover the forearms. Perform all procedures in the fume hood. Know the locations of the SDS, HF first aid kit, acid spill kit, emergency shower, and eye wash station.**
14. Obtain the HF manufacture container from the acid storage cabinet and pour 9mL into the 30mL PP HF storage beaker. This should be enough for creation of the electrolytes.
15. Replace the HF container in the acid storage cabinet.
16. At this stage there should only be 9mL of HF in the fume hood.
17. Create the etching electrolyte and the detachment electrolyte (note 1 & note 2).
18. Place the wafer in a 30mL PP beaker and use a PE pipet to transfer 1mL of the etching electrolyte to the beaker. Allow the wafer to sit in the solution for approximately 15 seconds. This will remove the native oxide layer and leftover organic residue.
19. Remove the wafer with HF resistant tweezers and hold over the incidental HF rinse bucket. Thoroughly rinse the wafer with ethanol 3 times ensuring the waste solution falls into the incidental HF rinse bucket.
20. Place the wafer on a Kim-wipe (the wafer will be dried with the air gun after the solutions have been disposed, so the neoprene gloves do not have to be repeatedly removed).
21. Place the 1mL of etching electrolyte used to clean the wafer in the 30mL PP HF waster beaker

<u>*Securing the silicon wafer in the etch cell*</u>

1. *Steps 1-10 require only nitrile gloves and can occur outside the fume hood.*
2. Tape the Al contact to the base of the etch cell, ensuring the tape will not cover the surface of the Al in contact with the Si wafer. The remaining length of Al should hang off the side of the etch cell base.
3. Place the top half of etch cell upside down and place O-ring in groove.
4. Place the wafer onto the O-ring ensuring the polished side is in contact with the O-ring.
5. Place the base of etch cell on top of the wafer ensuring the Al contact covers the wafer.

6. Gently hold the cell together to rotate right-side-up and then carefully screw halves together.
7. Fill cell with 2mL of ethanol and wait for 5 minutes.
8. Slide a Kim-wipe between cell halves and check for leaks indicating a poor seal.
9. Use a pipet to remove the ethanol from the etch cell to a 30mL PP beaker. Pour the solution in the beaker into the **solvent waste** container.
10. Use the air gun to dry the inside of the etch cell.

Electrochemically etching the wafer

1. *Steps 2-46 occur in the fume hood with appropriate PPE.*
2. **Handling HF is particularly hazardous and thus requires extensive safety precautions. Before working with HF, notify a coworker and instruct them to routinely check on you. Post a sign on the lab door when HF is being used. Wear long sleeved clothing and closed toe shoes. Wear a rubber apron, safety glasses, and face shield. Additionally, wear nitrile gloves inside neoprene gloves which cover the forearms. Perform all procedures in the fume hood. Know the locations of the SDS, HF first aid kit, acid spill kit, emergency shower, and eye wash station.**
3. Place the leak free etch cell in the HF resistant enclosure.
4. Use a PE pipet to transfer 3 mL of the etching electrolyte to the etch cell.
5. Ensure the Pt spiral electrode is clamped to the support stand and lower until the spiral portion is submersed in the electrolyte. Ensure the electrode does not touch the wafer.
6. Attach the negative (black) alligator clip to the end of the Pt electrode and attached the positive (red) alligator clip to the Al contact.
7. Rest arms inside the sink within the fume hood and gradually slide the neoprene gloves off, without touching the outside of the gloves. The gloves should remain in the sink.
8. Then, with only the nitrile glove on, deliver a constant current density of 90 mA/cm^2 for 300 seconds. This corresponds to a current of 108 mA for the etch cell which has an exposed area of 1.2 cm^2.
9. During this process observe the etch cell and ensure bubbling and splashing does not occur from the reaction. If this occurs, turn the power supply off and step back from the fume hood.
10. Turn the power supply off.
11. Remove the Pt electrode from the electrolyte by raising its position on the support stand.
12. Use a PE pipet to remove the etching electrolyte from the etch cell to the 30mL PP HF waste beaker.
13. Rinse the inside of the etch cell three times with ethanol, pipetting the waste ethanol from each rinse into the incidental HF rinse bucket.
14. Use a PE pipet to transfer 3 mL of the detachment electrolyte to the etch cell.
15. Lower the Pt electrode until the spiral portion is submersed. Ensure the electrode does not touch the wafer.
16. Rest arms inside the sink within the fume hood and gradually slide the neoprene gloves off, without touching the outside of the gloves. The gloves should remain in the sink.
17. Then, with only the nitrile glove on, deliver a constant current density of 4.5 mA/cm^2 for 15 minutes. This corresponds to a current of 5.4 mA for the etch cell which has an exposed area of 1.2 cm^2.

18. During this process observe the etch cell and ensure bubbling and splashing does not occur from the reaction. If this occurs, turn the power supply off and step back from the fume hood
19. Turn the power supply off.
20. Remove the Pt electrode from the electrolyte by raising its position on the support stand.
21. Unclip the alligator clips from the electrodes and place them to the side.
22. Use a PE pipet to remove the detachment electrolyte from the etch cell to a 30mL PP HF waster beaker.
23. Pour the 30mL PP HF waste beaker into the **HF waste** container.
24. Rinse the inside of the etch cell with ethanol 5 times and then rinse the outside of the etch cell with ethanol 3 times. Perform rinses over the incident HF rinse bucket.
25. Rinse the entirety of the etch cell with water 3 times, over the incidental HF rinse bucket.
26. Rinse the Pt electrode, HF resistant tweezers, and 30mL beakers with water 3 times each over the incidental HF rinse bucket.
27. Rinse the PE pipets with water and squirt the rinse solution into the incidental HF rinse bucket. Dispose of the PE pipets in the physical waste bucket.
28. Pour the **incidental HF waste** rinse solution into the HF indicial waste container.
29. Then rinse the incidental HF waste bucket 3 times with water and pour in the **incidental HF waste** container.
30. Rest arms inside the sink within the fume hood and gradually slide the neoprene gloves off, without touching the outside of the gloves. Ensure the gloves are positioned so the inside will not get wet if the sink is turned on. The gloves should remain in the sink.
31. Then, with only the nitrile gloves on, close the HF waste container and the HF incidental waste container.
32. Turn the water tap on.
33. Then slide arms back into neoprene gloves and thoroughly rinse the gloves in the sink with running water.
34. Once the neoprene gloves are rinsed, slide arms out and hang to dry.
35. Turn the water tap off.
36. Rinse the inside of the sink, where the gloves were rested.
37. Inspect the apron and face shield for HF solution. If clean, hang in respective locations. If exposed to HF, put neoprene gloves back on and rinse affected area with water and hang to dry.
38. Use the air gun to dry the wafer on the Kim-wipe.
39. Remove the nitrile gloves without touching the outside of the gloves and discard in the physical waste bin.

Detaching the PS film from the substrate

1. *Steps 2-7 require only nitrile gloves and can occur outside the fume hood.*
2. Unscrew the etch cell and separate the halves.
3. Remove the wafer with tweezers.
4. Carefully use ethanol to rinse the PS film from the wafer into a 50mL Pyrex beaker. The force of the ethanol rinse should cause the film to detach from the substrate and float free. If the film does not detach completely, use tweezers to apply pressure to the edges of the wafer.

5. Use tweezers to remove the PS film from the ethanol solution and place in a separate 50mL Pyrex beaker containing 10mL of cyclohexane for 1 minute. Cyclohexane is used to reduce capillary forces that would be caused by ethanol evaporating from the pores.
6. Use tweezers to remove the PS film from the cyclohexane solution and place on a Kim-wipe and allow to air dry.
7. Dispose of the cyclohexane and ethanol solutions in the **solvent waste** container.

Note 1: The etching electrolyte is a 3:1 by volume aqueous HF (49%) : ethanol (200 proof) solution. Create the electrolyte with 6mL of aqueous HF (49%) and 2mL of ethanol (200 proof). First, pour approximately 9mL of HF from the storage container into a 30mL PP beaker. Then, pour approximately 15mL of ethanol from the storage container into the PE bottle with spout. Next, measure the required volume of ethanol using a 10mL Pyrex graduated cylinder and then pour the ethanol into 30mL PP beaker. Next, use a PE pipet to transfer HF to a 10 ml PP graduated cylinder until the required amount is measured. Then slowly pour the HF into the beaker containing the ethanol.

Note 2: The detachment electrolyte is a 3:46 by volume aqueous HF (49%) : ethanol (200 proof) solution. Create the electrolyte with 0.375mL of aqueous HF (48%) and 5.75mL of ethanol (200 proof). Use the excess HF and ethanol that was poured from the storage containers from note 1. Next, measure the required volume of ethanol using a 10mL Pyrex graduated cylinder and then pour the ethanol into 30mL PP beaker. Next, use a PE pipet to transfer HF to a 10 ml PP graduated cylinder until the required amount is measured. Then slowly pour the HF into the beaker containing the ethanol.

Operating Agilent E3648A power supply in constant current mode:

1. Connect load.
2. Turn on power supply.
3. Press HIGH under voltage range to set voltage limit to 20V.
4. Press DISPLAY LIMIT.
5. Adjust knob to voltage limit of 20V.
6. Press $\frac{\text{VOLTAGE}}{\text{CURRENT}}$.
7. Adjust knob to required current limit.
8. Press DISPLAY LIMIT.
9. Turn output ON.
10. Ensure power supply is in constant current mode by verifying the CC annunciator is lit.

Ultrasonic bath settings:

1. Ensure the bath is filled with adequate water to partially submerge the glass beaker.
2. Insert a 250mL beaker containing 20mL of IPA and the silicon wafer, into the bath.
3. Cover the beaker with para film.

4. Press POWER.
5. Press the SELECT OPTION arrow keys until SET SONICS is selected.
6. Wait 15 minutes until the display reads 45.
7. Remove the beaker and cover the top of the ultrasonic bath with aluminum foil/parafilm. This reduces water evaporation.

Figure 1: Fume Hood Material Location

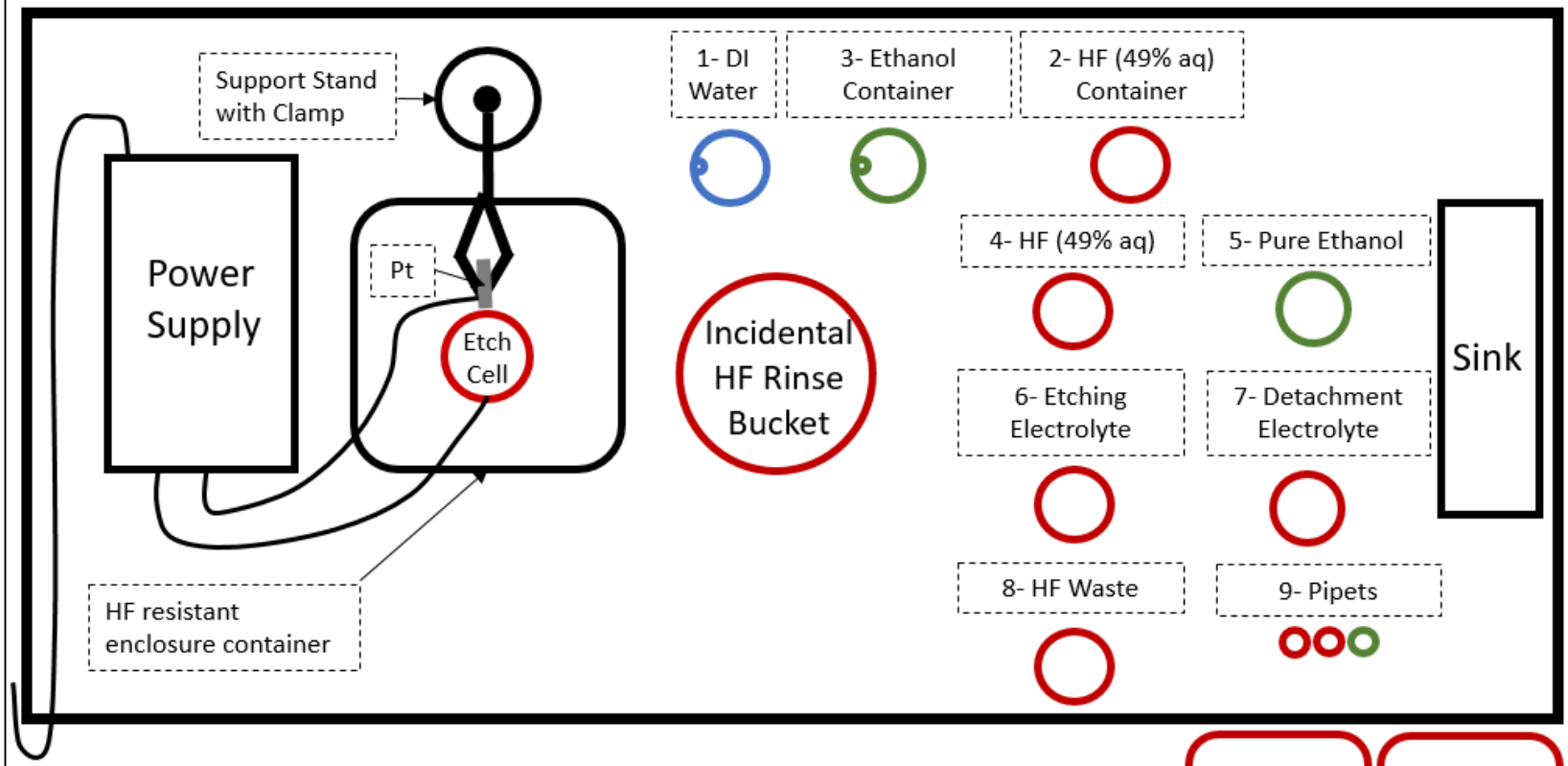

1,3 – PE bottle with spout
2 – Manufactures' bottle for HF
4, 5, 6, 7, 8 - 30mL PP Beaker
9 – Disposable Transfer Pipets PP or PE

Incidental HF Waste | Acid Waste
Solvent Waste | Physical Waste Bin

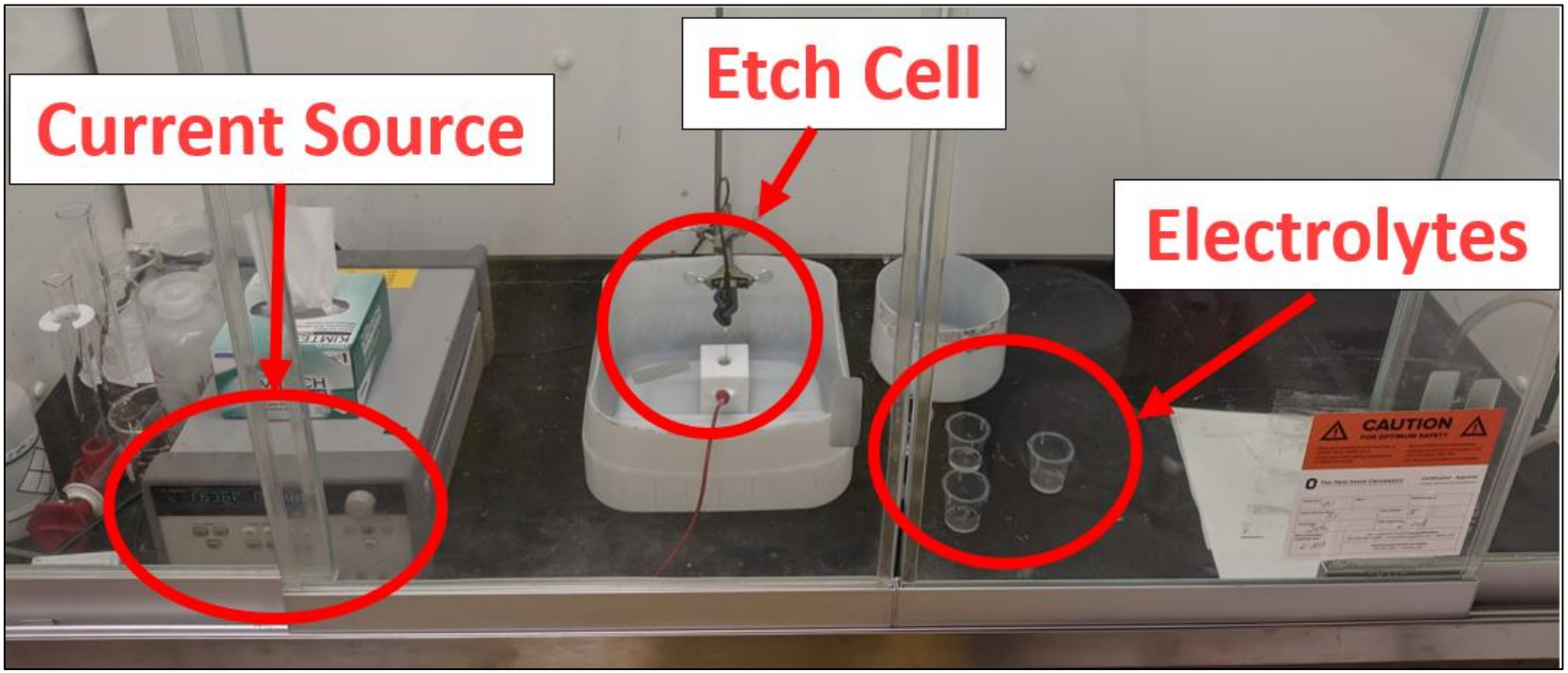
Current Source
Etch Cell
Electrolytes
CAUTION

Appendix B

Etch cell detailed drawings

Drawings on next page.

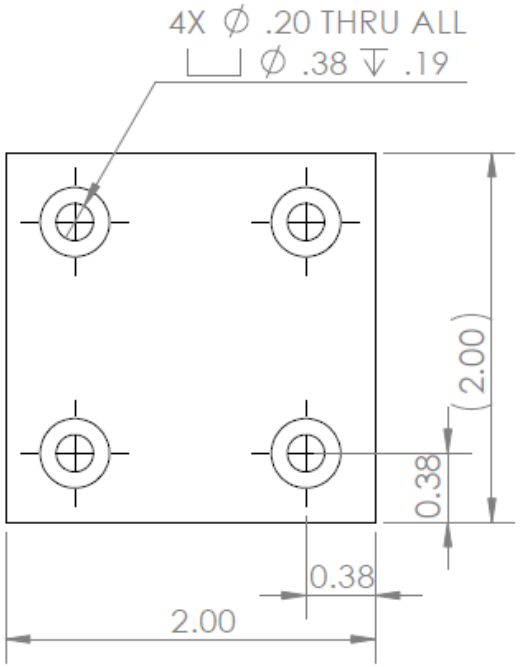

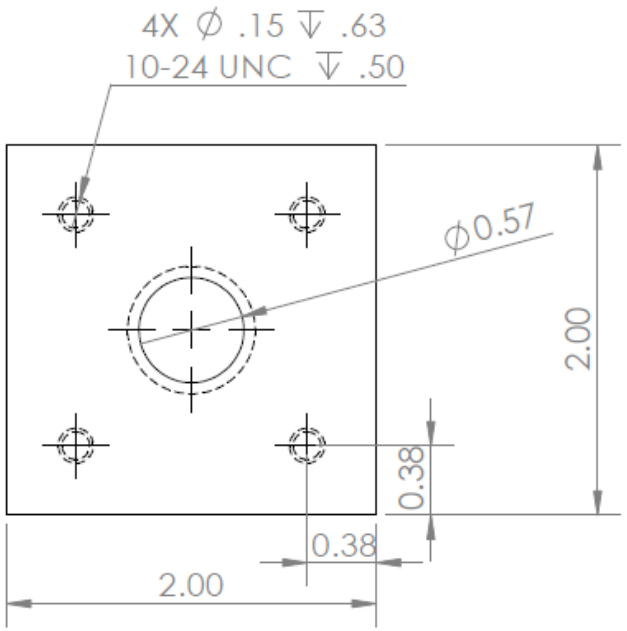

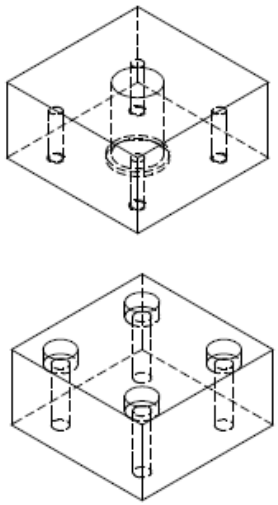

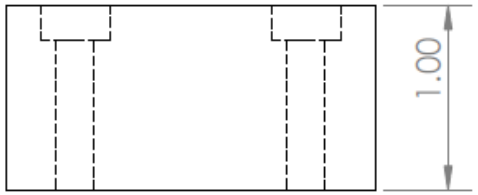

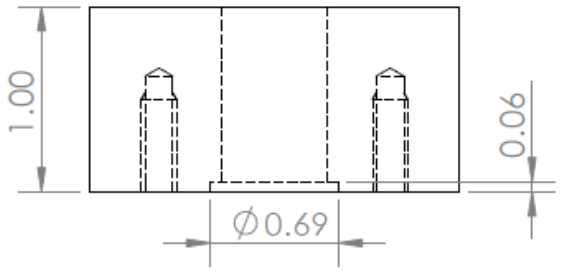

B2

		UNLESS OTHERWISE SPECIFIED:		NAME	DATE
		DIMENSIONS ARE IN INCHES TOLERANCES: FRACTIONAL ± ANGULAR: MACH ± BEND ± TWO PLACE DECIMAL ± THREE PLACE DECIMAL ±	DRAWN	J LAZENBY	01/08/2018
			CHECKED		
			ENG APPR.		
			MFG APPR.		
		INTERPRET GEOMETRIC TOLERANCING PER:	Q.A.		
		MATERIAL TEFLON	COMMENTS: DO NOT USE GLASS FILLED TEFLON		
NEXT ASSY	USED ON	FINISH			
APPLICATION		DO NOT SCALE DRAWING			

TITLE:

ETCH CELL

SIZE	DWG. NO.	REV
A		

SCALE: 1:1	WEIGHT:	SHEET 1 OF 1

Appendix C

Testing station detailed drawings

Drawings on next page.

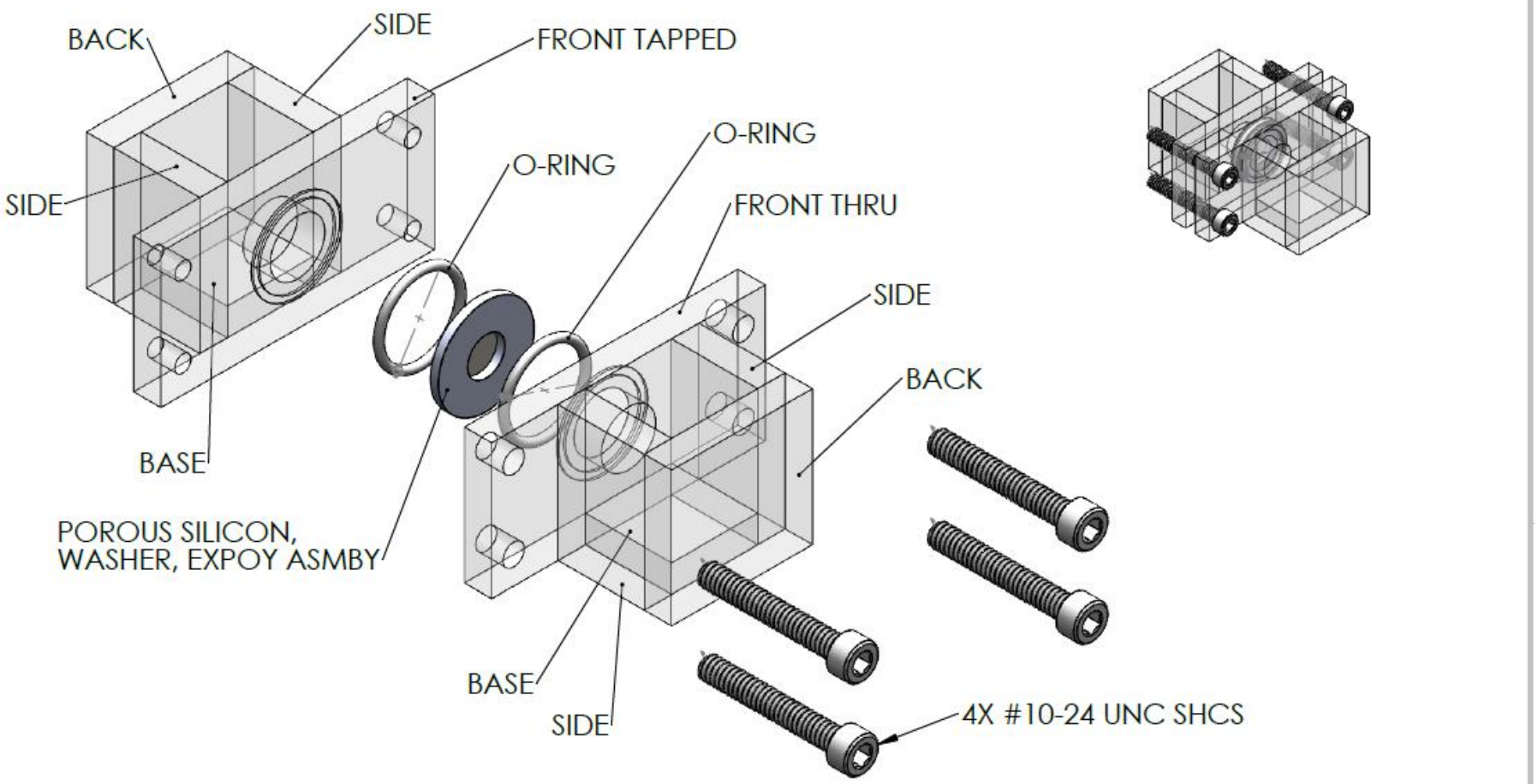

		UNLESS OTHERWISE SPECIFIED:		NAME	DATE
		DIMENSIONS ARE IN INCHES TOLERANCES: FRACTIONAL ± ANGULAR: MACH ± BEND ± TWO PLACE DECIMAL ± THREE PLACE DECIMAL ±	DRAWN	J LAZENBY	11/18/19
			CHECKED		
			ENG APPR.		
			MFG APPR.		
		INTERPRET GEOMETRIC TOLERANCING PER:	Q.A.		
		MATERIAL ACRYLIC 1/4"	COMMENTS:		
NEXT ASSY	USED ON	FINISH			
APPLICATION		DO NOT SCALE DRAWING			

TITLE:

TESTING STATION

SIZE	DWG. NO.	REV
A		

SCALE: 1:2	WEIGHT:	SHEET 1 OF 2

C2

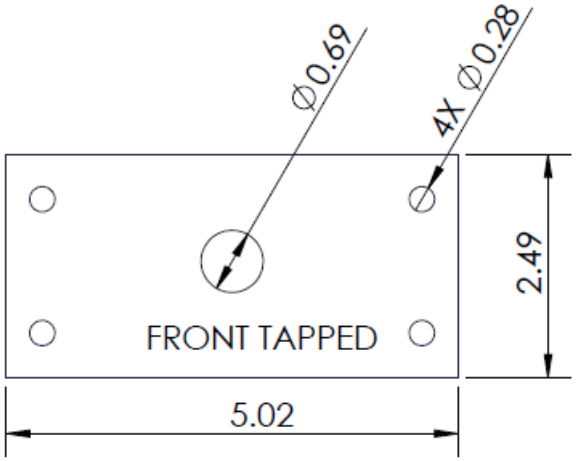

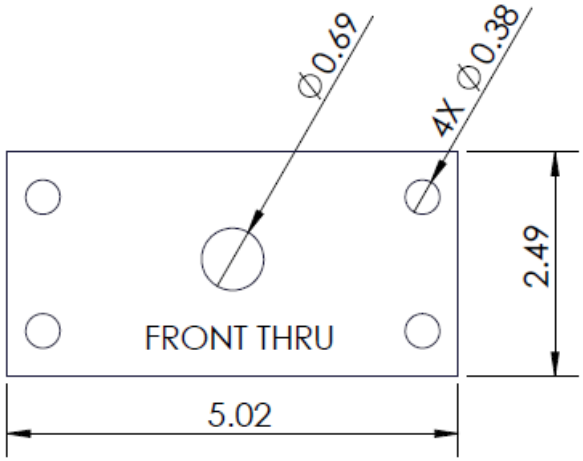

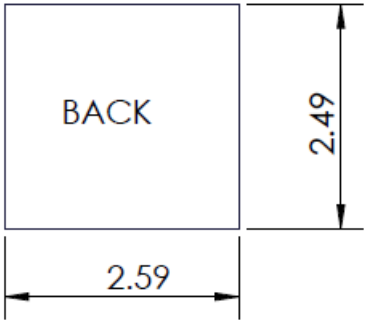

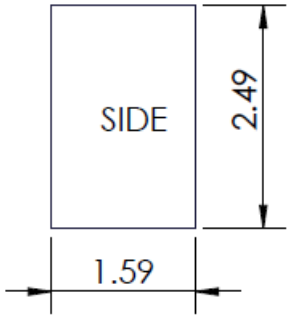

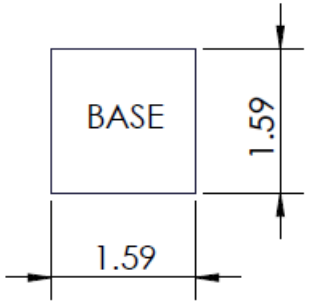

NOTES;

1) ALL DIMENSIONS TAKE INTO ACCOUNT FOCAL POINT OF LASER CUTTER

2) ALL SHEET IS 1/4IN THICK

3) ALL SIDES ARE BONDED USING WELD-ON 16

C3

		UNLESS OTHERWISE SPECIFIED:		NAME	DATE
		DIMENSIONS ARE IN INCHES TOLERANCES: FRACTIONAL ± ANGULAR: MACH ± BEND ± TWO PLACE DECIMAL ± THREE PLACE DECIMAL ±	DRAWN	J LAZENBY	11/18/19
			CHECKED		
			ENG APPR.		
			MFG APPR.		
		INTERPRET GEOMETRIC TOLERANCING PER:	Q.A.		
		MATERIAL ACRYLIC	COMMENTS:		
NEXT ASSY	USED ON	FINISH			
APPLICATION		DO NOT SCALE DRAWING			

TITLE:

TESTING STATION

SIZE	DWG. NO.	REV
A		

SCALE: 1:2	WEIGHT:	SHEET 2 OF 2

Appendix D

Spectrophotometer calibration data and instrument settings

Figure D1: UV – VIS instrument settings.

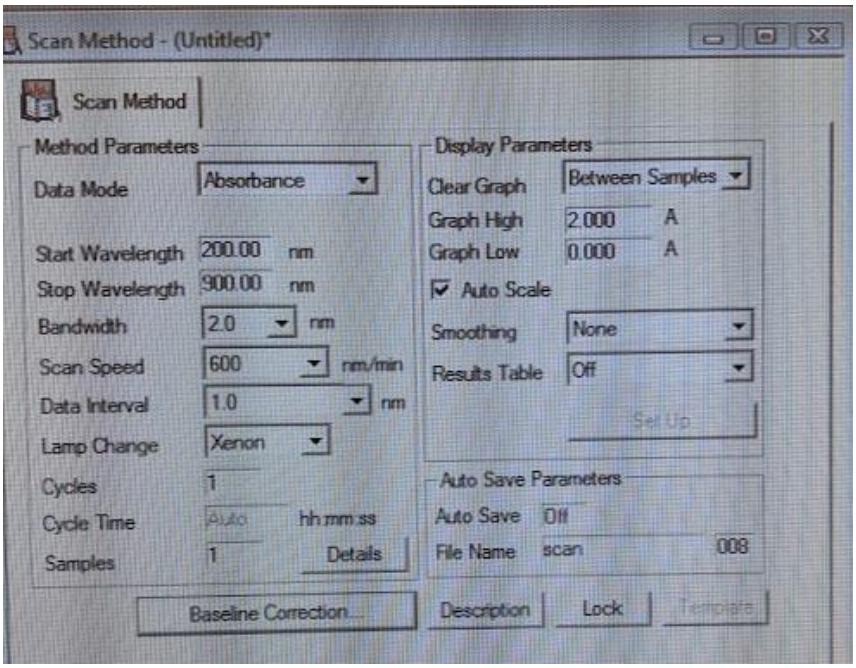

Figure D2: Absorption spectrum of MB at varying concentrations.

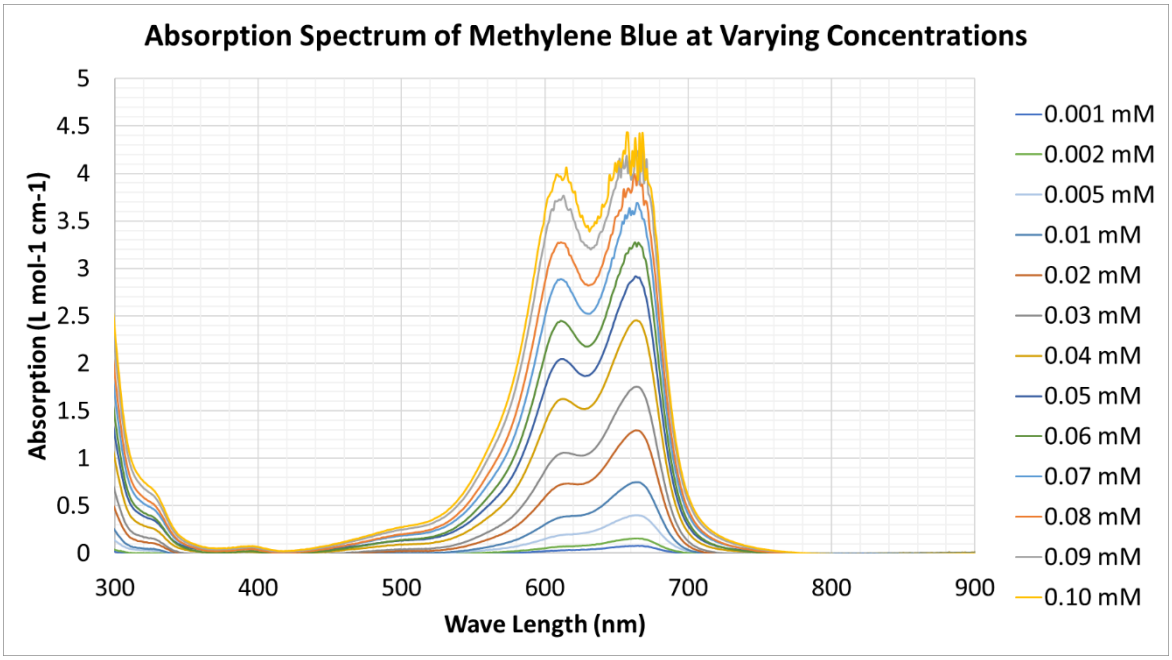

Table D1: Points used for absorption-concentration curve.

Molarity (mM)	Actual Molarity (resolution) (mM)	Absorptivity Value
0.001	0.001008263	0.08
0.002	0.001993037	0.157
0.005	0.004993997	0.4
0.01	0.01031713	0.745
0.02	0.019696339	1.291
0.03	0.030012869	1.758
0.04	0.040328986	2.452
0.05	0.04970782	2.912
0.06	0.060023336	3.229
0.07	0.070338441	3.688
0.08	0.079732844	3.878
0.09	0.090049411	4.183
0.10	0.100365566	4.154
0.20	0.200703031	4.584
0.50	0.500819713	NA

Appendix E

Etching logbook

Logbook for Practice Etches with 0.31 Ω-cm Wafer

		Pore Formation Etch		Film Detachment Etch			
Etch #	Date	Current Density (mA/cm^2)	Duration (m)	Current Density (mA/cm^2)	Duration (m)	Lift Off Result	What Happened to Membrane
1	1/17/2018	90	5	5	2	Unable to lift off	Practice
2	1/19/2018	90	5	6	10	Fragments of Si in electrolyte	Practice
3	1/25/2018	90	5	4	5	Fragments of Si in electrolyte	Practice
4	1/29/2018	90	5	10	2	Unable to lift off	Practice

Logbook for Etches with 0.001-0.005 Ω-cm Wafer -- before comprehensive recording

		Pore Formation Etch		Film Detachment Etch			
Etch #	Date	Current Density (mA/cm^2)	Duration (m)	Current Density	Duration (m)	Lift Off Result	What Happened to Membrane
5	2/2/2018	90	5	5	2	No Lift Off	Unable to lift off
6	2/3/2018	90	5	6	4.5	75%	Used for SEM - blurry image
7	2/11/2018	90	5	4	6.5	Fragmented Lift Off	Used for SEM - blurry image
8	2/24/2018	90	5	3	15	75%	Broke during handling
9	2/26/2018	90	10	2.5	20	25%	Unable to lift off
10	2/27/2018	290	5	2.5	20	25%	Unable to lift off

Logbook for Etches with 0.001-0.005 Ω-cm Wafer -- after comprehensive recordings and observations								
		Pore Formation Etch						
Etch #	Date	Electrolyte Composition - aq HF(48%):Ethanol (v/v)	Set Current (mA)	Actual Current (mA)	Actual Current Density (mA/cm^2)	Observed Voltage Initial (V)	Observed Voltage Final (V)	Duration (m)
11	3/17/2018	3:1	138	108	90	0.5	0.54	5
12	3/17/2018	3:1	138	108	90	0.69	0.71	5
13	3/18/2018	3:1	138	108	90	0.61	0.64	5
14	3/20/2018	3:1	138	108	90	0.57	0.62	5
15	9/11/2018	3:1	138	109	90.83333333	0.58	0.62	5
16	9/25/2018	3:1	138	108	90	0.58	0.62	5
17	9/28/2018	3:1	138	109	90.83333333	0.58	0.62	5
18	10/11/2018	3:1	138	108	90	0.59	0.65	5
19	10/16/2018	3:1	138	108	90	0.62	0.66	5
20	10/31/2018	3:1	138	108	90	0.62	0.66	5
21	1/8/2019	3:1	138	108	90	0.52	0.56	5
22	1/9/2019	3:1	138	108	90	0.55	0.57	5
23	1/10/2019	3:1	138	108	90	0.48	0.53	5
24	1/12/2019	3:1	138	108	90	0.53	0.57	5
25	1/15/2019	3:1	138	108	90	0.64	0.68	5
26	1/17/2019	3:1	138	108	90	0.57	0.60	5
27	1/18/2019	3:1	138	108	90	0.58	0.62	5
28	1/25/2019	3:1	138	108	90	0.63	0.66	5
29	2/12/2019	3:1	138	108	90	0.61	0.65	5
30	2/13/2019	3:1	138	108	90	0.56	0.6	5
31	2/14/2019	3:1	138	108	90	0.58	0.62	5
32	2/18/2019	3:1	138	108	90	0.59	0.63	5
33	2/19/2019	3:1	138	108	90	0.62	0.66	5
34	2/20/2019	3:1	138	108	90	0.57	0.61	5
35	3/4/2019	3:1	138	108	90	0.6	0.64	5
36	3/5/2019	3:1	138	108	90	0.57	0.6	5

Logbook for Etches with 0.001-0.005 Ω-cm Wafer -- after comprehensive recordings and observations

	Film Detachment Etch							
Etch #	Electrolyte Composition - aq HF(48%):Ethanol (v/v)	Set Voltage (V)	Actual Voltage (V)	Current Initial (mA)	Observed Current Final (mA)	Average Actual Current Density (mA/cm^2)	Duration (m)	Bath to Detach?
11	2:22	19	16.35	7	8	6.25	4.5	No
12	2:22	6	5.19	8	8	6.666666667	6	No
13	2:22	19	16.35	5	6	4.583333333	4.5	No
14	3:21	19	16.35	25	23	20	4.5	No
15	NA	NA	NA	NA	NA	NA	NA	No
16	NA	NA	NA	NA	NA	NA	NA	No
17	1:23	19	16.36	3	4	2.916666667	15	No
18	1:23	19	NA	NA	NA	NA	NA	No
19	1:23	19	16.36	3	4	2.916666667	17.5	Yes
20	1:23	RAMP UP	15.5	5	5	4.166666667	14	Yes
21	1:23	RAMP UP	16.36	5	5	4.166666667	15	Yes
22	1:23	RAMP UP	16.36	3	4	2.916666667	15	Yes
23	1:23	RAMP UP	16.35	3	5	3.333333333	16	Yes
24	1:23	RAMP UP	16.35	2	3	2.083333333	15	Yes
25	3:46	RAMP UP	16.35	3	4	2.916666667	15	Yes
26	3:46	RAMP UP	16.35	5	6	4.583333333	15	Yes
27	3:46	RAMP UP	16.35	6	7	5.416666667	15	Yes
28	3:46	RAMP UP	16.35	5	6	4.583333333	15	Yes
29	3:46	RAMP UP	16.35	6	7	5.416666667	15	Yes
30	3:46	RAMP UP	16.35	5	1	2.5	15	Yes
31	3:46	RAMP UP	16.35	4	5	3.75	15	Yes
32	3:46	RAMP UP	16.35	5	6	4.583333333	15	Yes
33	3:46	RAMP UP	16.35	2	3	2.083333333	15	Yes
34	3:46	RAMP UP	16.35	5	6	4.583333333	15	Yes
35	3:46	RAMP UP	16.35	6	7	5.416666667	15	Yes
36	3:46	RAMP UP	16.35	3	5	3.333333333	15	Yes

Logbook for Etches with 0.001-0.005 Ω-cm Wafer -- after comprehensive recordings and observations			
Etch #	Lift Off Result	What Happened to Membrane	Notes
11	50%	Used for SEM - Instrument setting was incorrect	Seemed as though film had not completely detached, recommend loner detachment etch
12	No Lift Off	Issue during etch	Possible issue with detachment electrolyte, when 19V applied, current was 0.025mA.
13	50%	Used for SEM - Instrument setting was incorrect	Interesting since lower current density that Etch #7 but better liftoff
14	Fragmented	Unable to lift off	Initially, film seemed intact and that it would come off whole. Small amount of bubbles during detachment, implying HF concentration might be too high.
15	No Lift Off	Unable to lift off	The detachment etch was not performed, so SEMs could be taken of pores still attached to substrate. This will determine if detachment was impacting pore geometry.
16	No Lift Off	Unable to lift off	The detachment etch was not performed, so SEMs could be taken of pores still attached to substrate. This will determine if detachment was impacting pore geometry.
17	90%	Unable to lift off	Difficulty removing membrane from substrate, but 90-100% was detached
18	No Lift Off	Issue during etch	Detachment Etch ended within 5s of start. Power supply did not go into constant current mode and the initial amperage was high (about 2.2A). Electrolyte started to bubble heavily.
19	90-100%	Broke during handling	Water bath detachment worked really well. Still really fragile and difficult to remove without breaking
20	100%	Epoxied with acrylic to zinc	Ramped up initial voltage because when set to 19, circuit overloaded. Bath lift off worked extremely well. Was able to gently move from bath to Kim wipe.
21	90%	Broke during testing	After 24 hours, still attached to substrate, but seems ready to detach. Membrane broken into two pieces when being removed from water bath.
22	90%	NF Diffusion Testing	Membrane detached fine, but formation etch voltage might have been too low.
23	95%	Weld-on to zinc washer	Membrane detached very well.
24	75%	Weld-on to Acrylic -	Membrane did not detached by itself and required some prodding. Most likely because the detachment current density was low.
25	100%	Epoxied to zinc washer	Membrane detached very well. Detachment electrolyte had increased ratio of HF to raise current density and ease with detachment process.
26	90%	F Diffusion Testing	Membrane detached very well, but current density during detachment might have been too high and resulted in structural weakness which lead to crack.
27	93%	Epoxied with acrylic to zinc	Majority of membrane detached. Edges are brown in color which could be due to silicon dioxide remaining from the detachment etch
28	100%	Broke during testing	Detachment etch had average current density of past experiment. Lift-off went very well.
29	98%	Broke during functionalization	Most of membrane detached. Again, there was brownness around the edges, which could be caused by silicon dioxide
30	100%	Conductivity Diffusion testing	Current was very low during the detachment etch and possible something went wrong. However the lift-off was very good.
31	95%	NF Diffusion Testing	Current was again low during detachment, but majority of membrane detached.
32	98%	F Diffusion Testing	Membrane detached well, slight brownness around the edges
33	95%	Broke during handling	Membrane detached well but broke during removal from water bath. Detachment current was low
34	100%	NF Diffusion Testing	Prefect membrane detachment.
35	95%	NF Diffusion Testing	Good membrane detachment, again, slight brownness around edge. Detachment etch current was relatively high
36	95%	F Diffusion Testing	Membrane detached well.

Appendix F

Forward osmosis calculations

Non-Functionalized

#	Date of Measurement	Date of Wafer Fabrication	Type	Test #	Initial Parameters: Source Side: Concentration of MB in Source (mM)	Initial Parameters: Source Side: Concentration of NaCl in Source (mM)	Initial Parameters: Source Side: Volume of Source (mL)	Initial Parameters: Permeate: Concentration of MB in Permeate (mM)	Initial Parameters: Permeate: Concentration of NaCl in Permeate (mM)	Initial Parameters: Permeate: Volume of Permeate Water (mL)	Duration (Hours)
1	2/23/2019	1/9/2019	Non-Functionalized	New	0.05	100	9	0	0	9	24
2	2/25/2019	2/14/2019	Non-Functionalized	1	0.05	100	9	0	0	9	24
3	2/28/2019	1/9/2019	Non-Functionalized	Reused	0.05	100	9	0	0	9	24
4	3/1/2019	2/14/2019	Non-Functionalized	2	0.05	100	9	0	0	9	24
5	3/6/2019	2/20/2019	Non-Functionalized	1	0.05	100	9	0	0	9	24
6	3/7/2019	2/20/2019	Non-Functionalized	2	0.05	100	9	0	0	9	24
7	3/7/2019	3/4/2019	Non-Functionalized	1	0.05	100	9	0	0	9	24
8	3/8/2019	3/4/2019	Non-Functionalized	2	0.05	100	9	0	0	9	24

Final Parameters: Source Side: Absorptivity of MB Blue in Source	Source Side: Concentration of MB in Source (mM)	Source Side: Concentration of NaCl in Source (mM)	Source Side: Volume of Source (mL)	Permeate: Absorptivity of MB Blue in Permeate	Permeate: Concentration of MB in Permeate (mM)	Permeate: Concentration of NaCl in Permeate (mM)	Permeate: Volume of Permeate Water (mL)	Percent Reduction in Concentration	Percent Volume Lost	Precent Moles of MB Lost
1.943	0.037332608	74.6652154	8.8	0.099	0.001902176		8.8	25.3347846	2.22222222	23.2742
1.958	0.037620816	75.2416324	8.8	0.351	0.006744079		8.8	24.7583676	2.22222222	13.24198
2.011	0.038639153	77.2783058	8.8	0.134	0.002574663		8.8	22.7216942	2.22222222	19.40409
2.006	0.038543083	77.0861668	8.8	0.372	0.007147571		8.9	22.9138332	1.66666667	10.49055
1.896	0.036429554	72.8591088	8.8	0.451	0.008665469		8.8	27.1408912	2.22222222	11.81418
1.956	0.037582388	75.1647768	8.7	0.393	0.007551063		8.8	24.8352232	2.77777778	12.57419
1.974	0.037928239	75.8564772	8.8	0.271	0.005206967		8.8	24.1435228	2.22222222	15.64671
2.025	0.038908148	77.816295	8.8	0.292	0.005610459		8.8	22.183705	2.22222222	12.94139
							AVERAGE:	24.25400273	2.22222222	14.92341

Functionalized

#	Date of Measurement	Date of Wafer Fabrication	Type	How Many Times Tested?	Initial Parameters						Duration (Hours)
					Source Side			Permeate			
					Concentration of MB in Source (mM)	Concentration of NaCl in Source (mM)	Volume of Source (mL)	Concentration of MB in Permeate (mM)	Concentration of NaCl in Permeate (mM)	Volume of Permeate Water (mL)	
1	2/24/2019	1/17/2019	Functionalized	1	0.05	100	9	0	0	9	24
2	2/26/2019	1/17/2019	Functionalized	2	0.05	100	9	0	0	9	24
3	3/12/2019	2/18/2019	Functionalized	1	0.05	100	9	0	0	9	24
4	3/13/2019	2/18/2019	Functionalized	2	0.05	100	9	0	0	9	24
5	3/12/2019	3/5/2019	Functionalized	1	0.05	100	9	0	0	9	24
6	3/13/2019	3/5/2019	Functionalized	2	0.05	100	9	0	0	9	24

Final Parameters										
Source Side				Permeate						
Absorptivity of MB Blue in Source	Concentration of MB in Source (mM)	Concentration of NaCl in Source (mM)	Volume of Source (mL)	Absorptivity of MB Blue in Permeate	Concentration of MB in Permeate (mM)	Concentration of NaCl in Permeate (mM)	Volume of Permeate Water (mL)	Percent Reduction in Concentration	Percent Volume Lost	Precent Moles of MB Lost
2.589	0.049744787	99.4895742	9	0.122	0.002344096		8.7	0.5104258	1.66666667	4.021493
2.572	0.049418151	98.8363016	8.7	0.089	0.001710037		8.7	1.1636984	3.33333333	1.15217
2.479	0.047631258	95.2625162	8.8	0.094	0.001806107		8.8	4.7374838	2.22222222	3.322487
2.498	0.047996322	95.9926444	8.8	0.107	0.002055887		8.8	4.0073556	2.22222222	2.120124
2.533	0.048668809	97.3376174	8.9	0.105	0.00201746		8.8	2.6623826	1.66666667	0.201342
2.564	0.04926444	98.5288792	8.8	0.098	0.001882962		8.8	1.4711208	2.22222222	0.021586
							AVERAGE:	2.425411167	2.22222222	1.806534